Gravitational wave background produced by a network of cosmic strings generated during a primordial inflationary phase

Guilherme Luís de Sousa Fialho Guedes
Mestrado em Física
Departamento de Física e Astronomia
2018

Orientador
Pedro Pina Avelino, Professor Auxiliar, Faculdade de Ciências da Universidade do Porto

Coorientador
Lara Rodrigues da Costa Gomes de Sousa, Investigadora, Centro de Astrofísica da Universidade do Porto

Todas as correções determinadas pelo júri, e só essas, foram efetuadas.

O Presidente do Júri,

Porto, _____/_____/_____

Gravitational wave background produced by a network of cosmic strings generated during a primordial inflationary phase

Guilherme Luís de Sousa Fialho Guedes

Supervisor: Pedro Pina Avelino

Co-supervisor: Lara Sousa

A Thesis presented for the degree of

Master of Physics

in the

Faculdade de Ciências da Universidade do Porto
Departamento de Física e Astronomia

October 2018

Acknowledgements

I would firstly like to thank Pedro Avelino and Lara Sousa for guiding through the development of this thesis. Thank you for always being available to answer my many doubts and introducing me to the topic.

I would also like to thank Jorge, for being a true friend, and Maria for motivating me to be the best version of myself and for the continuous encouragement through this period.

Last but not least, I want to thank my parents for allowing me to pursue my goals.

Abstract

Gravitational wave background produced by a network of cosmic strings generated during a primordial inflationary phase

by

Guilherme Luís de Sousa Fialho Guedes

Cosmic strings are linelike topological defects at the cosmological scale. They are predicted by several theories to be formed during the evolution of the Universe as the result of phase transitions. Cosmic strings are expected to produce cosmological signatures which would allow their detection, one of which being the production of a Stochastic Gravitational Wave Background (SGWB). In this work we compute this gravitational wave background generated by a network of cosmic strings for a wide range of parameters. To do so, the velocity-dependent one scale model was used to describe the evolution of a cosmic string network.

We focused on the case in which a cosmic string network is produced during an inflationary stage in the early Universe — which we will refer to as an i-string network. These networks are expected to enter a transient stretching regime during inflation, in which their characteristic length grows to scales larger that the Hubble radius. After inflation ends, the network eventually attains the standard evolution after re-entering the Hubble volume. However, during the stretching regime, emission of gravitational waves is significantly suppressed and, therefore, the SGWB power spectrum produced by i-strings exhibits a high-frequency signature on an otherwise standard spectrum. We argue that, if observed by current or forthcoming gravitational wave experiments, this signature would provide strong evidence for the existence of i-strings, and for a (primordial) inflationary phase.

We have also developed an algorithm for the quick computation of the SGWB generated by i-strings from that of a standard cosmic string network. Given that current observational constraints may be evaded by this i-string signature, this algorithm may be useful in revising such constraints and obtaining them for future experiments.

Resumo

Fundo de ondas gravitacionais produzida por uma rede de cordas cósmicas gerada durante a fase inflacionária primordial

por

Guilherme Luís de Sousa Fialho Guedes

Cordas cósmicas são defeitos topológicos a uma dimensão espacial à escala cosmológica. Várias teorias prevêm que elas se formem durante a evolução do Universo, como resultado de transições de fase. Prevê-se que as cordas cósmicas produzam assinaturas cosmológicas que permitiriam a sua deteção, uma das quais é a produção de um fundo estocástico de ondas gravitacionais. Neste trabalho calculamos este fundo de ondas gravitacionais gerado por uma rede de cordas cósmicas para vários parâmetros. Para isso, usamos o modelo VOS (Velocity-dependent One Scale) para descrever a evolução de uma rede de cordas cósmicas.

Focámo-nos no caso em que a rede de cordas cósmicas é criada durante um período de inflação no Universo primordial — que chamaremos de uma rede de cordas-i. Prevemos que estas redes entram num regime transiente em que são esticadas durante a inflação, e o comprimento característico da rede aumenta para escalas maiores que o raio de Hubble. Quando a inflação termina, a rede eventualmente atinge a evolução padrão após reentrar no volume de Hubble. Contudo, enquanto não entram no volume de Hubble, a emissão de ondas gravitacionais pela rede é suprimida e por isso, o espectro de fundo estocástico de ondas gravitacionais produzido por cordas-i exibe uma assinatura específica a altas frequências. Argumentamos que, se esta assinatura for observada por experiências de deteção de ondas gravitacionais, seria uma forte indicação da existência de cordas-i e de uma fase primordial de inflação.

Desenvolvemos também um algoritmo para a computação rápida do espectro de ondas gravitationais gerado por i-strings a partir de um espectro standard. Dados que os constrangimentos atuais podem ser evadidos por esta assinatura de cordas-i, este algoritmo pode ser útil na revisão desses constrangimentos e na sua obtenção para experiências futuras.

Contents

List of Figures

List of Abbreviations

SGWB . . . . . Stochastic Gravitational Wave Background

VOS . . . . . Velocity-dependent One Scale

CMB . . . . . Cosmic Microwave Background

FRW . . . . . Friedmann-Robertson-Walker

LSS . . . . . Last Scattering Surface

GW . . . . . Gravitational Wave

LIGO . . . . . Laser Interferometer Gravitational wave Observatory

LISA . . . . . Laser Interferometer Space Antenna

SKA . . . . . Square Kilometer Array

VEV . . . . . Vacuum Expectation Value

Chapter 1

Introduction

Several grand unified scenarios predict the formation of topological defects at the cosmological scale, as a result of a symmetry-breaking associated with a phase transition [1]. The fact that a field can acquire different vacua states in different regions of the Universe upon the phase transition may lead to the formation of cosmological defects [2]. Nambu (1996) [3] was amongst the first to predict this: "*If my view is correct, the Universe may have a kind of domain structure. In one part of the Universe you may have a preferred direction of the axis; in another part, the direction of the axis may be different.*"

Depending on the nature of the symmetry-breaking, different types of defects may form. Cosmic strings are line-like defects at the cosmological scale. They are particularly interesting since their energy density is expected to remain a constant fraction of the total energy density of the Universe, instead of dominating it — as is the case of monopoles (point-like defects) for example [4].

Cosmic strings are predicted to generate specific signatures on cosmological observables, namely the production of a stochastic gravitational wave background (SGWB). The recent direct detection of gravitational waves (GWs) in 2015 [5] has opened the possibility of detecting this SGWB. In fact, future GWs experiments, such as LISA, have the prospect of either observing the SGWB produced by cosmic strings or tightening current constraints on string tension and other model parameters [6].

This GW signature is a consequence of cosmic strings interactions — either with themselves or with other cosmic strings — which may result in the creation of closed loops. These loops

oscillate under their tension and decay, emitting gravitational radiation. Since the production of these loops is predicted to occur throughout cosmological history, they are expected to give rise to a characteristic SGWB spectrum [7, 8, 9].

One of the main aims of this thesis was the development of an algorithm for the computation of the SGWB spectrum produced by a cosmic string network. We have applied this to the case in which a network is produced during an inflationary phase, which we will refer to as an i-string network for simplicity. The accelerated expansion of the Universe induces a stretching regime during which the production of loops and consequent emission of gravitational waves are suppressed. This results in a specific signature on the SGWB spectrum which will be computed and characterized.

This thesis is organized as follows:

1. In the second chapter, standard cosmology is reviewed along with the inflationary paradigm.

2. Topological defects — their formation and structure — are introduced in the third chapter, including the conditions for the creation of a cosmic string network.

3. In the fourth chapter the evolution of a network of cosmic strings is studied using the Velocity-dependent One Scale (VOS) model.

4. The SGWB spectrum generated by a standard network of cosmic strings is computed in the fifth chapter. A standard network is one which is created in the early Universe, after inflation.

5. In the sixth chapter, the case of a network created during an inflationary era is explored. In particular, the specific signature this network generates in the SGWB spectrum is characterized. Moreover, an algorithm to produce this SGWB spectrum from a standard one is developed. The contents of this chapter are based on the work reported in Ref. [10].

6. The conclusions and prospects for future work are presented in the seventh and last chapter.

   Throughout this thesis, natural units are used with $c = \hbar = k_B = 1$, where c is the speed of light, $\hbar$ is the reduced Planck constant and k_B is the Boltzmann constant.

Chapter 2

Standard Cosmology

Standard cosmology relies on the Cosmological Principle, an assumption that states that the statistical properties of the Universe are the same everywhere and in any direction, implying an homogeneous and isotropic Universe. In other words, no cosmological position (including our own) or direction are preferred. This principle is only defined in a statistical sense for large scales. It is not valid on small scales, where the heterogeneity of the Universe can be easily observed.

There are extensive evidence for the isotropy and homogeneity of the Universe, the most compelling being the measurements of the Cosmic Microwave Background (CMB) radiation. These measurements have shown that all points in the sky are at the same average temperature, with deviations of the order of 1 part in 10^5 [11].

The notion that the Universe is expanding is also another pillar for standard cosmology. This discovery was made by Edwin Hubble in 1929 when he observed that distant galaxies were receding from Earth at velocities proportional to the distance. Since then, several experiences have confirmed this relation [12]. The fact that distant galaxies are moving away from us following a linear relation for their velocity (instead of moving in random directions), suggests that the Universe is expanding.

From this explanation, it follows that the physical — or proper — distance between two

comoving [1] observers, increases with physical time

$$d(t) = a(t)d(t_0)\,, \tag{2.1}$$

where $d(t)$ is the proper distance measured at time t and $d(t_0)$ the proper distance measured at present time t_0. The scale factor $a(t)$ is set to unity at present time, $a(t_0) = 1$.

Differentiating Eq.(2.1) with respect to time, one obtains the linear relation which was observed by Hubble,

$$\dot{d}(t) = \frac{\dot{a}(t)}{a(t)} d(t)\,, \tag{2.2}$$

where a dot represents derivation with respect to time. The proportionality parameter is called the Hubble parameter, $H = \dot{a}(t)/a(t)$.

The Hubble parameter is measured, at the present time, to be

$$H_0 = 100\,h\,\frac{km}{s\,Mpc}\,, \tag{2.3}$$

with $h = 0.679$ in accordance with the Planck data [13]. We adopt the convention of writing H_0 in terms of 'little h', h, in order to incorporate all the uncertainties into h.

Another implication of an expanding Universe is the redshifting of frequencies of gravitational waves. As was the case with proper distances, the expansion increases their wavelength, λ, which will lead to the decrease of the frequency, f, of emitted gravitational waves according to

$$\frac{f_{em}}{f_{obs}} = \frac{a(t_{obs})}{a(t_{em})}\,, \tag{2.4}$$

where the subscript em represents the time of emission and obs the time of observation. The redshift, z is defined as

$$z = \frac{\lambda_{obs} - \lambda_{em}}{\lambda_{em}}\,, \tag{2.5}$$

thus implying that $z = a(t_{obs})/a(t_{em}) - 1$.

[1] Comoving means that it is moving with the expansion of the Universe

2.1 General Relativity

The dynamics of expansion of the Universe, namely the evolution of the scale factor, is described by the Einstein equations:

$$G_{\mu\nu} \equiv R_{\mu\nu} - \frac{1}{2} g_{\mu\nu} R = 8\pi G T_{\mu\nu} - \Lambda g_{\mu\nu} \,, \tag{2.6}$$

where $G_{\mu\nu}$ is the Einstein tensor, $R_{\mu\nu}$ is the Ricci tensor, $g_{\mu\nu}$ is the metric, R is the Ricci scalar, G is the gravitational constant, $T_{\mu\nu}$ is the stress-energy tensor and Λ is the cosmological constant, which may also be interpreted as the energy of the vacuum.

The Ricci scalar is calculated from the contraction of the Ricci tensor with the metric, $R = g^{\mu\nu} R_{\mu\nu}$, and contracting the first and third indices of the Riemann curvature tensor, one gets the Ricci tensor, $R_{\mu\nu} = R^{\rho}_{\mu\rho\nu}$. The Riemann curvature tensor is defined as:

$$R^{\rho}_{\sigma\mu\nu} = \Gamma^{\rho}_{\nu\sigma,\mu} - \Gamma^{\rho}_{\mu\sigma,\nu} + \Gamma^{\rho}_{\mu\lambda}\Gamma^{\lambda}_{\nu\sigma} - \Gamma^{\rho}_{\nu\lambda}\Gamma^{\lambda}_{\mu\sigma} \,, \tag{2.7}$$

where

$$\Gamma^{\sigma}_{\mu\nu} = \frac{1}{2} g^{\sigma\alpha} (g_{\mu\alpha,\nu} + g_{\alpha\nu,\mu} - g_{\mu\nu,\alpha}) \tag{2.8}$$

are the Christoffel symbols, which are the components of the torsion-free and metric-compatible connection in general relativity.

The assumption of isotropy and homogeneity implies the absence of heat conduction and viscosity. It can then be considered that the cosmological background behaves as a perfect fluid, for which the stress-energy tensor is written as:

$$T^{\mu\nu} = (p + \rho) u^{\mu} u^{\nu} - p g^{\mu\nu} \,, \tag{2.9}$$

where ρ and p are, respectively, the energy density and pressure of the fluid and u^{μ} is the normalized 4-velocity, $u^{\mu} u_{\mu} = 1$. In the comoving frame, since the fluid is at rest, one has $u^0 = 1$ and $u^i = 0$.

Eqs. (2.6) can be solved using the Friedmann-Robertson-Walker (FRW) metric, which follows from the isotropy and homogeneity of an expanding Universe. This metric yields the

following line element:

$$ds^2 = dt^2 - a^2(t)\left[\frac{dr^2}{1-\kappa r^2} + r^2(d\theta^2 + \sin\theta d\phi^2)\right], \tag{2.10}$$

where r, θ and ϕ are comoving coordinates and κ is a curvature paramenter of the 3-dimensional space. This parameter can take different values, depending on the topology of the Universe:

- $\kappa > 0$ for a spherical Universe, also called a closed Universe;
- $\kappa = 0$ for a flat Universe;
- $\kappa < 0$ in the case of an hyperbolic Universe, or an open Universe.

Let us introduce an alternative time coordinate, the conformal time τ, which will be useful in future sections, defined as

$$d\tau = \frac{dt}{a(t)}\,. \tag{2.11}$$

Using the FRW metric and the stress-energy tensor of a perfect fluid, Eq. (2.9), to solve the Einstein equations, Eq. (2.6), results in the Friedmann equations:

$$H^2 = \frac{8}{3}\pi G\rho - \frac{\kappa}{a^2} - \frac{\Lambda}{3}\,, \tag{2.12}$$

$$-2\frac{\ddot{a}}{a} - \frac{\dot{a}^2}{a^2} - \frac{\kappa}{a^2} + \Lambda = 8\pi G p\,. \tag{2.13}$$

These equations allow for the description of the dynamics of the expansion of the Universe based on its contents and curvature.

2.2 Universe contents

From the Einstein equations, Eq. (2.6), the covariant conservation of the Einstein tensor [14]— which can be derived from the Bianchi identity — and metric-compatibility imply that the stress-energy tensor is also covariantly conserved, $T^{\mu\nu}{}_{;\nu} = 0$, representing the momentum and energy conservation in curved spacetime. The $\mu = 0$ component of the covariant conservation

of the stress-energy tensor yields the equation of continuity for the energy density:

$$\dot{\rho} + 3\frac{\dot{a}}{a}(\rho + p) = 0\,. \tag{2.14}$$

Considering a linear equation of state, $p = w\rho$, where w is the equation-of-state parameter, Eq. (2.14) can be solved to obtain the evolution of the energy density with the scale factor. In the case of a constant w, it results in

$$\rho \propto a^{-3(1+w)}\,. \tag{2.15}$$

The observable Universe is usually considered to be comprised by three different components with contributions to the energy density of the background: matter (ρ_m), radiation (ρ_r) and the vacuum energy density (ρ_Λ). Given the different rates of dilution with the scale factor due to their different equations of state, each component dominates the evolution of the Universe at different cosmological times. The period of time dominated by a specific component is usually called an era. The radiation, matter and vacuum energy (Λ) eras are illustrated in Fig. (2.1), where a_{eq} represents the value of the scale factor at the instant when the energy densities of matter and radiation are equivalent and a_Λ marks the moment when the energy density of the vacuum becomes dominant.

Each of these components satisfies the equation of continuity, Eq. (2.14). To calculate the cosmological evolution of the energy density of each component, the equation-of-state parameter, w, is necessary. For the case of non-relativistic matter, $w = 0$, and therefore, from Eq. (2.15),

$$\rho_m \propto a^{-3}\,. \tag{2.16}$$

For radiation, $w = 1/3$, following that

$$\rho_r \propto a^{-4}\,. \tag{2.17}$$

For the case of the vacuum energy density, $w = -1$, and ρ_Λ remains constant throughout cosmological history. Therefore, as observed in Fig. 2.1, an expanding Universe which results in the dillution of ρ_r and ρ_m eventually becomes dominated by the constant vacuum energy

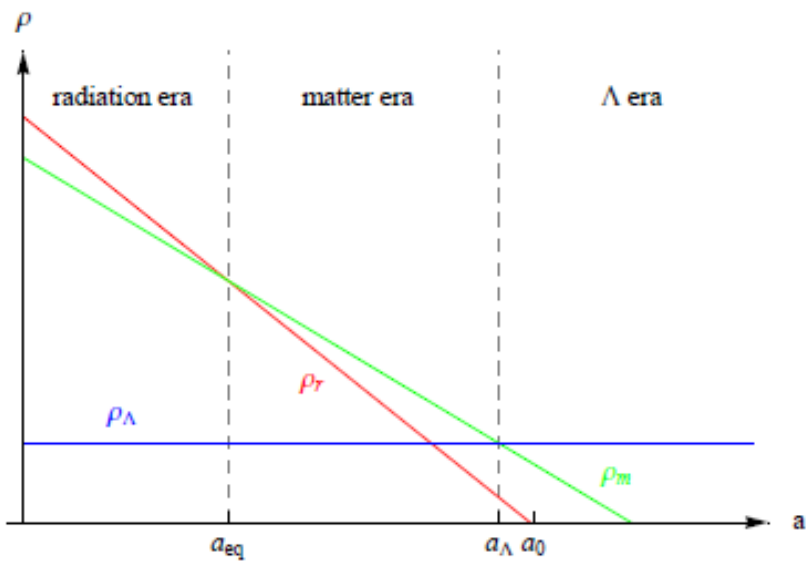

Figure 2.1: The evolution of the energy density of the 3 components of the background energy density throughout cosmological history. Radiation (ρ_r) is depicted in red, while matter (ρ_m) is illustrated in green and the vacuum energy density (Λ) is in blue. The vertical dashed lines indicate the separation between the different eras, a_{eq} represents the moment when radiation and matter contributions becomes equivalent and a_Λ the instant when the vacuum energy density dominates. a_0 corresponds to the scale factor today [15].

density.

Another important quantity is the critical density, ρ_c, which is defined as the energy density corresponding to a flat ($\kappa = 0$) Universe. Absorbing the energy density of the vacuum into the energy density of the background ($\rho \to \rho - \frac{\Lambda}{8\pi G}$ and $p \to p + \frac{\Lambda}{8\pi G}$) the critical density can be written as

$$\rho_c = \frac{3H^2}{8\pi G}\,, \tag{2.18}$$

by setting $\kappa = 0$ in the first Friedmann equation, Eq. (2.12).

It is common to normalize the energy density of each component of the Universe with respect to the critical density at a specific time, defining the dimensionless density parameter:

$$\Omega_i \equiv \frac{\rho_i}{\rho_c}\,, \tag{2.19}$$

where the index i indicates the different components that contribute to the total energy density

of the cosmological background. The Friedmann equation, Eq.(2.12), can be written as:

$$\Omega = \sum_i \Omega_i = 1 - \Omega_\kappa \,, \tag{2.20}$$

where $\Omega_\kappa = -\kappa/(aH)^2$. The value of Ω determines the value of κ. For a closed Universe, with $\kappa > 0$, $\Omega > 1$; an open Universe, with $\kappa < 0$, has $\Omega < 1$; a flat Universe, with $\kappa = 0$, leads to $\Omega = 1$. The relative energy density at the present time has been measured to be $\Omega_0 = 1.000 \pm 0.005$ from the Planck observations [13], indicating a flat Universe. Given that $\Omega = 1$ is a repeller solution (for radiation and matter dominated Universes) and the enormous timescale of cosmological evolution, a Universe with Ω slightly different than unity would quickly depart from a flat one. Therefore, the fact that current observations place this value so close to unity seems to be a strong indication that we can take $\kappa = 0$.

With the assumption of a flat Universe, Eq. (2.12) can be solved to give the evolution of the scale factor with cosmological time, taking into account Eq. (2.15):

$$a = \left(\frac{t}{t_0}\right)^{\frac{2}{3(1+w)}} \,, \tag{2.21}$$

where we considered $a(t_0) = 1$. This equation is valid for a constant $w \neq -1$. It is common to write $a \propto t^\beta$ which results in $H = \beta/t$.

Substituting with the respective w, we get $a \propto t^{1/2}$ for a radiation dominated Universe and $a \propto t^{2/3}$ for a matter dominated one. In the case of the energy density of the vacuum, $w = -1$, the scale factor does not evolve according to Eq. (2.21), but to $a = a_0 \exp(H_0 t)$ and the Hubble parameter is a constant.

The Friedmann equation, Eq (2.12), can be written in terms of observable parameters at the present time:

$$\frac{H^2}{H_0^2} = \Omega_{0,r} a^{-4} + \Omega_{0,m} a^{-3} + \Omega_{0,k} a^{-2} + \Omega_{0,\Lambda} \,, \tag{2.22}$$

where the subscript 0 corresponds to the values of the parameters at the present time. The values that are used in this work are in accordance with the Plank data [13]: $\Omega_{0,r} = 2.47 \times 10^{-5} h^{-2}$, $\Omega_{0,\Lambda} = 0.694$, $\Omega_{0,k} = 0$ and $\Omega_{0,m} = 1 - \Omega_{0,r} - \Omega_{0,\Lambda}$.

2.3 Cosmological horizons

To determine the causal structure of spacetime, one must study how photons move in a FRW Universe since the speed of light imposes a limit to how fast information can be transmitted. Photons travel along null geodesics, with $ds^2 = 0$. Considering a photon propagating through space in a radial direction, with θ and ϕ remaining constants, we get that, in a flat Universe, along the path of the photon,

$$dr = \frac{dt}{a} = d\tau \,. \tag{2.23}$$

The computation of the maximum distance a photon can travel since the beginning of time, t_i, allows for the determination of which regions of the Universe are causally connected at time t. This distance is called the particle horizon, d_H, and distances greater than d_H at time t imply causally disconected regions: they could not have yet communicated. Considering that the Universe has a finite age, photons can only travel a finite distance until time t:

$$d_H = a(t) \int_{t_i}^{t} \frac{dt'}{a(t')} \,. \tag{2.24}$$

For radiation or matter dominated Universes, $d_H \propto t$.

The event horizon, on the other hand, measures how far a photon can travel from time t until the maximum time in the future, t_{max}, determining regions of space with which one will never be in causal contact with. It is calculated as:

$$d_e(t) = \int_{t}^{t_{max}} \frac{dt'}{a(t')} \,. \tag{2.25}$$

For models where the Universe recollapses, there is a t_{max} and therefore there will be an event horizon since Eq. (2.25) converges for a matter, radiation or vacuum energy dominated Universe. Otherwise, for a Universe which does not recollapse, the upper bound of the integral becomes $+\infty$ and d_e is ∞ for a matter or radiation dominated flat Universe; there is no event horizon meaning that we would be able to send light signals to every part of the Universe eventually. However, in a Universe dominated by the vacuum energy density, Λ — which data suggests is the case currently — one gets that $d_e \simeq H_0^{-1}$. This means that there is an event horizon and consequently, parts of the Universe that we will never see.

Despite not being a cosmological horizon, H^{-1}, also called the Hubble radius, is an interesting distance. From Eq. (2.2), it can be determined that the recessional velocity of an object distant by one Hubble radius is $\dot{d}(t) = H(t)H^{-1}(t) = 1$. This implies that objects outside of the Hubble sphere (at a distance greater than the Hubble radius) recede from us at a superluminal velocity.

This does not mean that we cannot send light signals to these objects. In fact, it was just mentioned that, for a radiation or matter dominated Universe, there is no event horizon. This is so because the Hubble radius increases (faster than the expansion rate of the Universe) in these cases, $H^{-1} = t/\beta$ — with $\beta = 1/2$ for a radiation dominated Universe and $\beta = 2/3$ for matter domination. Therefore, the Hubble radius eventually becomes greater than the distance to these far away objects, which will then recede at a subluminal velocity. However, in a Λ dominated Universe, H^{-1} is constant, and consequently, every object outside of the Hubble sphere will never be in causal contact with us. This is in agreement with the result of the event horizon for a Λ dominated Universe, $d_e = H^{-1}$.

The comoving Hubble radius is defined as $(aH)^{-1}$. It is important to note the difference between the comoving Hubble radius and the comoving particle horizon, $\tau = \int_{t_i}^{t} \frac{dt'}{a(t')}$: if two comoving objects are distanced more than the comoving horizon, this means that they could never have communicated with each other; however, if they are separated by more than $(aH)^{-1}$, this means that they are receding from each other at superluminal velocities now — it is possible that they were causally connected in the past.

2.4 Shortcomings of Standard Cosmology

Standard cosmology successfully explains many aspects of the observable Universe — many of which we did not mention — such as the Hubble expansion, the abundance of light elements or the cosmic microwave background radiation. However, one must assume a very particular initial state with some apparently inexplicable features, in order to, using standard cosmology, arrive at the present Universe.

We will mention three of the problems that have been identified in standard cosmology: the horizon problem, the flatness problem and the monopole problem.

2.4.1 The horizon problem

As mentioned before, CMB measurements have shown that all points in the sky have similar temperatures, with very slight deviations. The homogeneity and isotropy that is observed today implies that the photons which have travelled in our direction were roughly at the same temperature at the time of the last scattering. [2] For this to be true, one would expect them to be emitted by regions causally connected at that time, otherwise there does not seem to be an apparent reason for this homogeneity, since these regions could not have yet communicated.

Within the framework of standard cosmology, the comoving Hubble radius increases monotonically throughout radiation or matter dominated eras,

$$(aH)^{-1} \propto t^{1-\beta} = t^{\frac{1+3w}{3(1+w)}} , \tag{2.26}$$

meaning that the largest scales we see today are only now coming into causal contact.

This problem can be quantified by looking at Fig. 2.2. At the time of last scatering, the causally connected regions were, at most, separated by a comoving distance, τ_{LSS}.

Considering that $\tau_0 \gg \tau_{LSS}$, where τ_0 is the conformal time at the present, one can calculate the angle which τ_{LSS} would correspond to in today's sky, assuming a flat Universe, as:

$$\tan(\theta/2) \simeq \frac{\tau_{LSS}}{2\tau_0} = \frac{1}{2(1+z_{LSS})^{1/2}} , \tag{2.27}$$

where it was assumed that the Universe was dominated by matter.

The last scattering surface is predicted to have occured at $z \simeq 1100$, resulting in $\theta \sim 2^{\text{o}}$. However, the homogeneity we observe in the CMB spans a much larger region of angular space. In fact, this calculation corresponds to saying that the present Hubble volume contains 10^5 regions which were not causally connected at the time of the last scattering [16]. Therefore, unless we assume that these regions were at the same temperature to start with, standard cosmology does not offer an explanation to this homogeneity.

[2] The last scattering represents the moment when photon decoupling occurs. Afterwards photons propagate freely across the Universe without significant interactions with other particles, which is why the Universe is said to become transparent subsequently. Their temperature redshifts with expansion and yields a black body spectrum observed today.

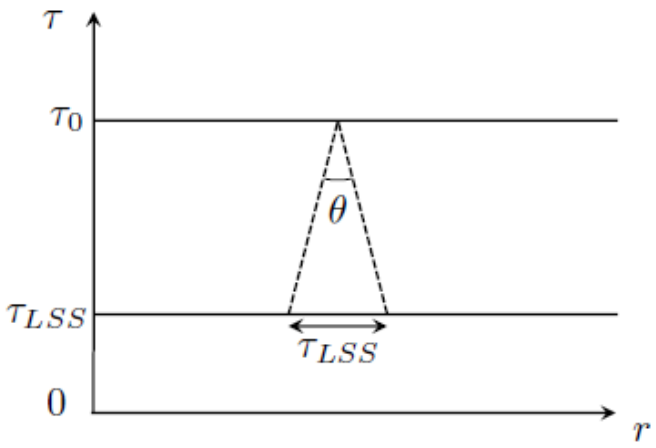

Figure 2.2: Spacetime diagram where the vertical axis represents conformal time, τ and co-moving distance is given by r in the horizontal axis. The angle θ represents the angular size of the particle horizon at the time of the last scattering in the present sky [15].

2.4.2 The flatness problem

This problem has to do with the apparent flatness of the present Universe. The Friedmann equation, Eq. (2.12), can be written in terms of Ω as

$$(\Omega^{-1} - 1) = -\frac{3}{8\pi G}\frac{k}{\rho a^2}\,. \tag{2.28}$$

For a radiation dominated Universe, $\Omega^{-1} - 1 \propto a^2$ and for a matter dominated one, $\Omega^{-1} - 1 \propto a$. This implies that a deviation from the $\Omega = 1$ at early times would grow as the Universe expands. As previously stated, the currently observed value for Ω is very close to unity. Therefore, in order for the present Universe to be so close to a flat one, the initial deviation from unity must be incredibly small. For instance, at Planck scale, [15]

$$|\Omega - 1| \lesssim 10^{-60} \tag{2.29}$$

to arrive at the current Universe.

Therefore, within standard cosmology, in order for the Universe to be as flat as presently observed, it must have had a very special set of initial conditions.

2.4.3 Monopole problem

As the Universe cools, it is expected to go through phase transitions which may lead to the formation of topological defects, as will be seen in detail in the next chapter. In particular, many theories of grand unification predict the production of monopoles [15], corresponding to an energy density that will typically dominate the Universe [4]. However, monopoles have yet to be observed, and standard cosmology does not provide a mechanism to avoid their production or any process capable of dilluting them.

2.5 A basic picture of inflation

These shortcomings seem to indicate the need for an adjustment to standard cosmology at early times. Let us start by exploring the horizon problem. It was noted that standard cosmology predicts a monotonically increasing comoving Hubble radius, meaning that scales coming into causal contact today have never been causally connected. Therefore, to solve the horizon problem, a mechanism that results in a decrease of the comoving Hubble radius is necessary. Such a mechanism could explain the observed homogeneity since, scales that are now coming into causal contact, could have been causally connected at some point in the early Universe. This mechanism is depicted in Fig. 2.3.

This mechanism may also be the solution for the flatness problem. If we rewrite Eq. (2.28) as

$$(\Omega - 1) = -\frac{k^2}{(aH)^2}\,. \tag{2.30}$$

we notice that a phase of decreasing $(aH)^{-1}$ would drive the Universe towards flatness, making $\Omega = 1$ an attractor solution to the Friedmann equations. Provided that the phase of decreasing comoving Hubble radius is sufficiently long, the initial conditions that result in the present Universe do not need to be as strict as in standard cosmology.

From Eq. (2.26), in order for the comoving Hubble radius to decrease, $-1/3 < w < -1$. The condition of $w < -1/3$ is also a condition for accelerated expansion,

$$\frac{d}{dt}\left(\frac{1}{aH}\right) < 0 \Leftrightarrow \frac{d^2a}{dt^2} > 0\,. \tag{2.31}$$

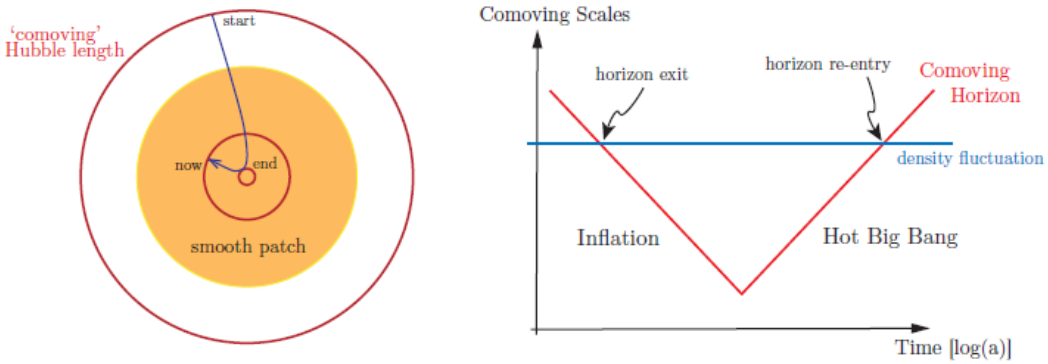

Figure 2.3: *Left*: Diagramatic evolution of the comoving Hubble radius, $(aH)^{-1}$. The blue arrow indicates the time direction of the evolution. From the start of inflation until its end, the comoving Hubble radius decreases; afterwards it will increase until the value observed today. This allows every region in the smooth patch to have been in causal contact before. *Right*: The evolution of the comoving Hubble radius with the logarithm of the scale factor. Again, during inflation $(aH)^{-1}$ decreases, increasing afterwards according to standard cosmology. Thus, cosmological scales that are now coming into causal contact may have been causally connected in the early Universe [17]

This period of accelerated expansion that solves the horizon and flatness problems is usually called inflation. It is predicted to have happened in the early Universe, preceding the era of radiation domination.

We have already encountered an example with $w = -1$, the vacuum energy. However, a Universe dominated by Λ could not be the solution since this energy density would not dillute with the scale factor (it is constant) and therefore radiation and matter domination epochs, predicted by standard cosmology, could not follow. This can be solved by considering that inflation is a transient phase, in which the energy density of the Universe is dominated by a fluid that behaves like Λ for a finite period of time and then decays.

This accelerated expansion also solves the monopole problem since it will dillute produced monopoles much more than predicted. This solution is only acceptable if one considers that monopoles are not produced after inflation ends.

2.6 Gravitational waves

Gravitational waves are perturbations of the metric of space-time, which propagate at the speed of light. They are the solution to Eqs. (2.6) after linearization under the weak-field

approximation. The weak-field approximation considers the metric $g_{\mu\nu}$ to be nearly the same as the Minkowski metric $\eta_{\mu\nu}$, suffering only a small perturbation, $h_{\mu\nu}$,

$$g_{\mu\nu} = \eta_{\mu\nu} + h_{\mu\nu}\,. \tag{2.32}$$

Given the Minkoswki metric, $\eta_{\mu\nu} = diag(-1, 1, 1, 1)$, a small perturbation means that $|h_{\mu\nu}| \ll 1$ and we can ignore terms of higher order than $\mathcal{O}(h^2)$. Using the metric from Eq. (2.32) the Einstein tensor becomes [14]:

$$\begin{aligned} G_{\mu\nu} &= R_{\mu\nu} - \frac{1}{2}\eta_{\mu\nu}R \\ &= \frac{1}{2}(\partial_\sigma\partial_\nu h^\sigma_\mu + \partial_\sigma\partial_\mu h^\sigma_\nu - \partial_\mu\partial_\nu h - \Box h_{\mu\nu} - \eta_{\mu\nu}\partial_\mu\partial_\nu h^{\mu\nu} + \eta_{\mu\nu}\Box h)\,, \end{aligned} \tag{2.33}$$

where $h = h^\mu_\nu$ is the trace of the perturbation and $\Box$ is the D'Alembertian for a flat spacetime, $\Box = -\partial_t^2 + \partial_x^2 + \partial_y^2 + \partial_z^2$.

To solve the linearized Einstein equations it is common to choose the harmonic gauge [14], corresponding to $g^{\mu\nu}\Gamma^\rho_{\mu\nu} = 0$, which in the weak field approximation becomes

$$\partial_\mu h^\mu_\lambda - \frac{1}{2}\partial_\lambda h = 0\,. \tag{2.34}$$

Introducing a more convenient quantity, the trace transversed perturbation, $\bar{h}_{\mu\nu} \equiv h_{\mu\nu} - \frac{1}{2}\eta_{\mu\nu}h$, the linearized Einstein equations simplify to

$$\Box\bar{h}_{\mu\nu} = -16\pi G T_{\mu\nu}\,, \tag{2.35}$$

and in the vacuum

$$\Box\bar{h}_{\mu\nu} = 0\,. \tag{2.36}$$

It follows then that the perturbation of the metric propagates as wave at the speed of light.

2.6.1 Sources of Gravitational Waves

The generation of gravitational waves by sources can be studied from Eq. (2.35), from which it can be shown that the produced trace-transversed perturbation is proportional to the

second derivative of the quadrupole moment tensor [14], q_{ij}, defined as

$$q_{ij}(t) = 3 \int x^i x^j T^{00}(t, \mathbf{x}) d^3x \,. \tag{2.37}$$

In the case of eletromagnetic radiation, the leading contribution comes from the changing dipole moment. On the other hand, gravitational waves do not possess dipolar radiation since a changing dipolar moment corresponds to a violation of momentum conservation [14, 18]. The main contribution is therefore quadrupolar. Monopole radiation does not exist in both cases due to charge and mass conservation.

The radiated power from a gravitational source follows from the quadrupole formula [14]

$$-\frac{dE_{GW}}{dt} = \frac{G}{45} \left\langle \frac{d^3 Q_{ij}}{dt} \frac{d^3 Q_{ij}}{dt} \right\rangle , \tag{2.38}$$

where Q_{ij} is the traceless part of the quadrupole moment,

$$Q_{ij} = q_{ij} - \frac{1}{3} \delta_{ij} \delta^{kl} q_{kl} \,. \tag{2.39}$$

Some typical sources of gravitational waves include objects orbiting each other and spinning non-axisymmetric objects. In general an accelerated motion which is neither spherically symmetric (spherically pulsating star) nor an axisymmetric rotation (rotating disk), will have a non-zero second time derivative of the quadrupole moment and emit gravitational radiation.

2.6.2 Stochastic Gravitational Wave Background

A stochastic gravitational wave background (SGWB) is a signal that is usually produced by a large amount of weak sources scattered through the Universe. The stochastic aspect of the signal stems from the fact that it is characterized statistically. These signals are usually broadband, which means that they cover a wide range of frequencies. Unlike burst sources, where a particular event produces GWs (such as a supernova explosion), or periodic signals (like binary systems), SGWBs are continuously present throughout the cosmological history of the Universe.

There are several possibles sources of a SGWB. For instance, associated to inflation, to

phase transitions in the early Universe or to cosmic strings [19]. The SGWB produced by a network of cosmic strings is the object of study of this thesis. Unlike other possible sources, cosmic strings, if they exist, may still be actively emitting today, despite the fact that cosmic string networks are expected to be produced in the early Universe.

It is common to characterize the SGWB spectrum using Ω_{GW}, which is defined as the energy density in gravitational waves, ρ_{GW}, per logarithmic interval of frequency, normalized by the critical density at the present time, Eq. (2.18):

$$\Omega_{GW} = \frac{1}{\rho_c} \frac{d\rho_{GW}}{d\log f} \,. \tag{2.40}$$

The observational window for some gravitational waves experiments — both current or forthcoming experiments — is presented in Fig. 2.4. As we will see later, some of these may probe the SGWB spectrum produced by cosmic strings, allowing for their detection or further constraining of current models.

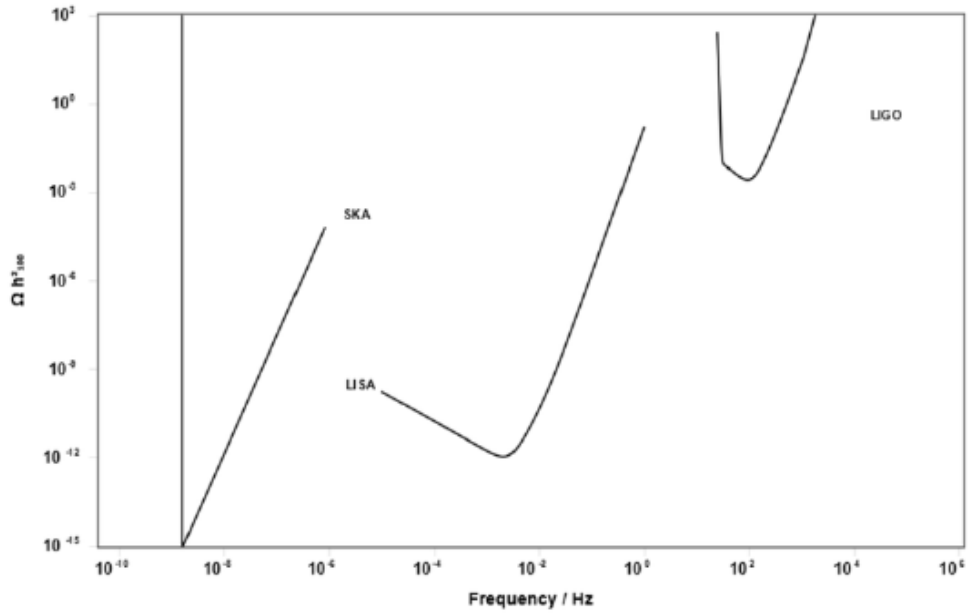

Figure 2.4: The observational window of three gravitational wave (GW) detection experiments: LIGO (Laser Interferometer Gravitational-Wave Observatory), an earth-bound gravitational wave detector, responsible for the first direct detection of gravitational waves; LISA (Laser Interferometer Space Antenna) a space-bound GW detector planned to be launched in 2034; SKA (Square Kilometre Array) a multi radio telescope project planned to start observations in 2022 [20].

Chapter 3

Topological defects

Cosmic strings are linelike topological defects at the cosmological scale. In this chapter the formation and structure of generic cosmological defects are introduced. Topological defects occur when a field develops a configuration which cannot be continuously deformed into the vacuum solution, resulting in a region of trapped energy. Despite the fact that they are predicted by several theories, and expected to be created due to spontaneous symmetry breaking associated with a cosmological phase transition [1, 2], topological defects have yet to be detected in the cosmological context.

We start by introducing the concept of spontaneous symmetry breaking within the framework of a model which would result in the production of cosmic strings.

3.1 Spontaneous symmetry breaking

Spontaneous symmetry breaking takes place when a system ends up in a state (for instance the vacuum state) which is not left invariant by the symmetries associated with the Lagrangian of the system. This concept can be illustrated using the Goldstone model with a single scalar complex field, ϕ, with the classical Lagrangian density, $\mathcal{L}$, defined as

$$\mathcal{L} = \partial_\mu \bar{\phi} \partial^\mu \phi - V(\phi)\,, \tag{3.1}$$

where the potential, $V(\phi)$, is

$$V(\phi) = \frac{1}{4}\lambda(\bar{\phi}\phi - \eta^2)^2\,, \tag{3.2}$$

where λ and η are positive constants. This model possesses global a $U(1)$ symmetry: the Lagrangian density, Eq. (3.1), remains invariant under global transformations of the $U(1)$ group:

$$\phi(x) \to e^{i\alpha}\phi(x)\,. \tag{3.3}$$

The symmetry is global since α is a constant.

The potential from Eq. (3.2) corresponds to the "mexican hat" potential and is depicted in Fig. 3.1. It is characterized by having a circle of minima, where $|\phi| = \eta$. Therefore, the vacuum state of this theory corresponds to the field ϕ taking a value in this circle, $\phi = \eta e^{i\theta}$, where θ is an arbitrary phase, corresponding to a specific position in the circle of minima.

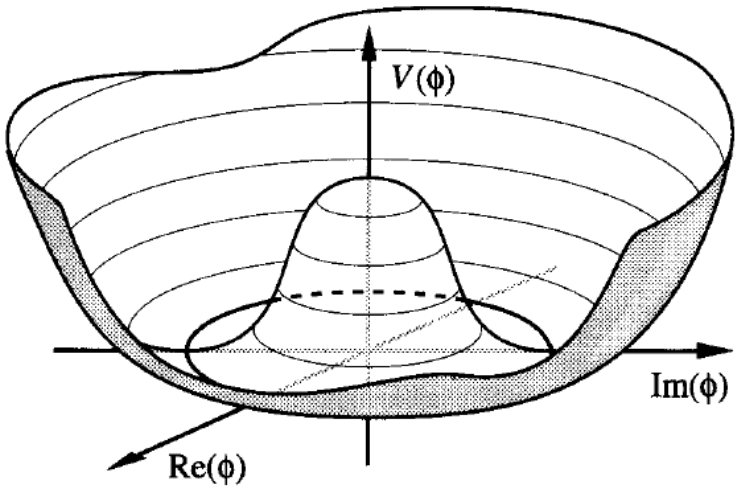

Figure 3.1: The "mexican hat" potential from Eq. (3.2), characterized by having a circle of minima and a relative maximum at the origin [1].

However, once the field acquires this VEV (vacuum expectation value), transformations of the $U(1)$ group, Eq. (3.3), do not leave the ground state invariant, since they result in a change of the phase θ into $\theta + \alpha$. This transformation keeps the value of the field in the circle of minima, but in a different position. The theory mantains its invariance, but the state does not. When this occurs, a spontaneous symmetry breaking is said to have happened.

3.2 Cosmological phase transitions

Throughout its evolution, as it cooled, the Universe is expected to have undergone phase transitions. Each phase transition occurs at a critical temperature, T_c, and is usually associated with a spontaneous symmetry breaking. For finite-temperature quantum field theory, the potential from Eq. (3.2) is replaced by an effective potential, which is equivalent to the free energy density [1]. Assuming that the chemical potentials of all particle species are vanishing, the free energy F is

$$F = E - TS\,, \tag{3.4}$$

where E is the internal energy, T the absolute temperature and S the entropy. The equilibrium value of ϕ is the one which minimizes Eq. (3.4). Given the dependence of the effective potential on the temperature, it may develop different minima as the Universe cools. In general, at high temperatures, the field takes a value of zero. Once it develops a non-zero value to minimize the effective potential, at a critical temperature T_c, the Universe is said to have undergone a phase transition.

An example of a second-order phase transition can be realized in the context of the Goldstone model of Eq. (3.1) with a high-temperature effective potential of the form [1]

$$V_{eff}(\phi, T) = \frac{\lambda}{12}(T^2 - 6\eta^2)|\phi|^2 + \frac{\lambda}{4}|\phi|^4\,, \tag{3.5}$$

where the ϕ-independent terms were omitted. For high temperatures the coefficient of $|\phi|^2$ is positive and the expectation value of the field is $\langle\phi\rangle = 0$. The field is in its symmetric state. However, for $T < \sqrt{6}\eta$, the coefficient is negative and the value of the field that minimizes the effective potential becomes different than 0; the field develops a non-zero expectation value. The value of $|\phi|$ which minimizes the effective potential is then

$$|\phi| = \frac{1}{\sqrt{6}}(T_c^2 - T^2)^{1/2}\,, \tag{3.6}$$

where $T_c = \sqrt{6}\eta$ is the critical temperature. When the temperature reaches this T_c a phase transition happens. Consequently, as the field takes a non-zero expectation value, Eq. (3.6), it is no longer in its symmetric state and so, a spontaneous symmetry breaking occurs.

The evolution of the shape of the effective potential with the temperature is depicted in Fig. 3.2, where it can be seen that for temperatures above the critical temperature the potential has only one minimum for $|\phi| = 0$ and for temperatures below the critical temperature, another minimum arises for a non-zero value of the field.

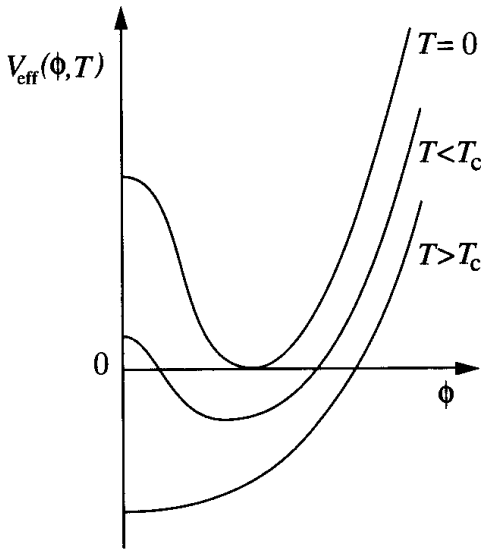

Figure 3.2: The evolution of the temperature-dependent effective potential for a second order phase transition [1].

From Eq. (3.6), when the field develops a non-zero VEV, only the modulus of ϕ is defined; the phase, θ, is left undefined. The choice of this phase depends on random fluctuations. Let us define the correlation length, $\xi(t)$, as the length above which the values of θ are uncorrelated. The specific value of the correlation length depends on the relaxation processes which are involved. Nonetheless, there is always an upper bound to the value of $\xi(t)$ due to causality constraints, since correlations cannot be established faster than the speed of light:

$$\xi(t) < d_H(t)\,. \tag{3.7}$$

Therefore, in regions of space which are causally disconnected at the time when the spontaneous symmetry breaking occurs, the phases of the field ϕ are uncorrelated. In other words, the field may develop distinct values in different regions of the Universe.

3.3 Topological defects formation

To study the formation and structure of topological defects, let us introduce the Goldstone model for a real scalar field with a Lagrangian density

$$\mathcal{L} = \partial_\mu \phi \partial^\mu \phi - V(\phi)\,, \tag{3.8}$$

where the potential is

$$V(\phi) = \frac{\lambda}{4}(\phi^2 - \eta^2)^2\,, \tag{3.9}$$

where λ and η are constants. This potential is represented in Fig. 3.3(a) and it possesses two degenerate minima, $\pm\eta$.

The Lagrangian density of Eq. (3.8) is invariant under transformations $\phi \to -\phi$ and therefore it has Z_2 symmetry. However, once the field develops an expectation value, $\pm\eta$, the Z_2 symmetry of the ground state is broken since these transformations do not leave it invariant — despite yielding a legitimate minimum of the potential.

Let us consider two cosmological regions which are separated by a larger distance than that of the correlation length associated with the symmetry breaking. In these two regions the field may develop different VEVs: for instance, $-\eta$ in the first region and η in the second one. The fact that the field develops different values in different regions corresponds to defining boundary conditions: $\phi(-\infty) = -\eta$ and $\phi(\infty) = \eta$. From Eqs. (3.8) and (3.9) with these boundary conditions one may arrive at [1]

$$\phi(x) = \eta \tanh\left(\sqrt{\frac{\lambda}{2}}\eta x\right), \tag{3.10}$$

which is the static solution of the field equations centered in $x = 0$.

In order to evolve continuously from a negative value to a positive one, a field with this configuration must take the value of zero somewhere, as illustrated in Fig. 3.3(b), which does not correspond to a minimum of the potential. Therefore, there is a region of space where the field is not in the true vacuum since it is not in the lowest energy state. Given that this configuration is not continuoulsy deformable into the true vacuum solution — which would correspond to the field only taking the value of η or $-\eta$ — a topological defect is formed.

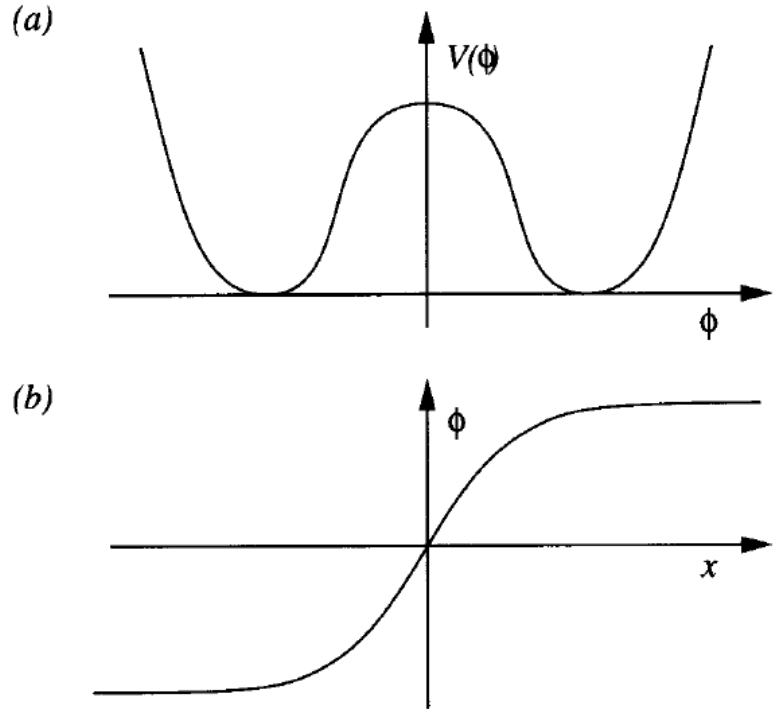

Figure 3.3: Top: The double-well potential from Eq. (3.9) with two minima. Bottom: The field solution Eq. (3.10) with boundary conditions $\phi(-\infty) = -\eta$ and $\phi(\infty) = \eta$. In order to continuously go from a negative value to a positive one, the field takes the value of 0 somewhere [1].

Extrapolating to 3 spatial dimensions, this gives rise to a thin surface which separates regions with different values of the field. This specific type of defect is called a domain wall. The thickness of the wall — the thickness of the region where the potential is significantly different from the minima — is approximately given by [1]

$$\delta \sim \eta^{-1}\sqrt{\frac{2}{\lambda}}\,. \tag{3.11}$$

Given the stability of this configuration, the topological defect becomes a region of trapped energy. In the case of an infinite domail wall, this energy is infinite, but its energy per unit of area is finite.

Let us go back to the Goldstone model for a complex field, Eqs. (3.1) and (3.2), in which a global $U(1)$ symmetry is broken. Following the same mechanism, the field in causally disconnected regions may develop VEVs with different phases, corresponding to different positions in

the circle of minima of the potential, Fig. 3.1. Therefore, it is possible for the field to adopt a configuration in which, as we transverse a closed path, $\Delta\theta = 2\pi$. An example of such a configuration is depicted in Fig. 3.4 , in which the field takes, for large r, the form of

$$\phi(r,\theta) \approx \eta e^{i\theta} \,. \tag{3.12}$$

However, at the center of the configuration, the phase of ϕ is not well defined. This can only be solved continuously if the field takes the value of 0, passing through the top of the potential in Fig. 3.4, which results in a region where the potential is not minimized.

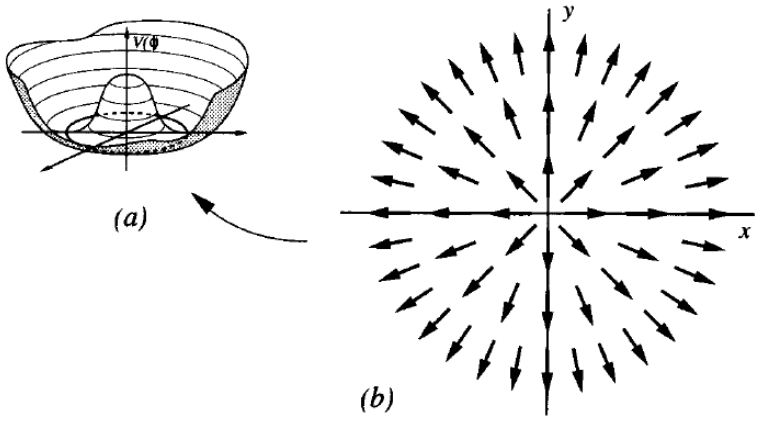

Figure 3.4: Left: "Mexican hat potential" with a circle of degenerate minima Right: Field configuration which results in the formation of a cosmic string since, by continuity, the phase of the field is not defined at the center [1].

This gives rise to a region of trapped energy which is not continuously deformed to the vacuum solution: it is a topological defect. In 3 spatial dimensions, it originates a line-like defect, called a cosmic string.

The energy density, ϵ, associated with the Lagrangian density of Eqs. (3.1) and (3.2) is

$$\epsilon = |\dot{\phi}|^2 + |\nabla\phi|^2 + V(\phi) \,. \tag{3.13}$$

To perform the area integral to calculate the energy density per unit lenght, μ, we define δ[1] as the radial distance from the center of the string until the point when the field is considered

[1]The estimation of the thickness of domain walls is also valid for cosmic strings [1]

to take the form of Eq. (3.12). Within a radial distance smaller than δ we will consider the field to be zero. Considering the time-independent string solution [1],

$$\mu \sim \frac{\pi}{4}\eta^4\lambda\delta^2 + \int_\delta^R \left[\frac{1}{r}\frac{\partial\phi}{\partial\theta}\right]^2 2\pi r dr \approx 2\pi\eta^2 \ln\left(\frac{R}{\delta}\right). \tag{3.14}$$

This result implies that the energy per unit length is divergent and a cut-off R is imposed to avoid it from becoming inifite. This cut-off depends on the physical situation and is usually provided by the distance to the nearest string. This divergence is not present when the broken symmetry is local.

The case of a broken local $U(1)$ symmetry happens for the Abelian-Higgs model with the following Lagrangian density:

$$\mathcal{L} = \bar{D}_\mu\bar{\phi}D^\mu\phi - V(\phi) - \frac{1}{4}F_{\mu\nu}F^{\mu\nu}\,, \tag{3.15}$$

where $D_\mu = \partial_\mu - igA_\mu$ is the covariant derivative, A_μ a gauge field, g the gauge coupling and $F_{\mu\nu} = \partial_\mu A_\nu - \partial_\nu A_\mu$. The potential is the same as in Eq. (3.2). This Lagrangian density is invariant under the $U(1)$ group of local gauge transformations,

$$\begin{aligned} \phi(x_\mu) &\to \phi(x_\mu)e^{i\alpha(x_\mu)}\,, \\ A_\mu(x_\mu) &\to A_\mu(x_\mu) - \frac{1}{g}\partial_\mu\alpha(x_\mu), \end{aligned} \tag{3.16}$$

where $\alpha(x_\mu)$ varies with the spacetime location (hence this represents a local symmetry).

In this case, for large r, both the scalar field and the gauge field contribute to the energy density, making it decrease exponentially fast for distances further than the thickness of the string. Consequently, the energy density per unit length of local cosmic strings is finite and approximately $\mu \sim \eta^2$ [1]. This linear energy density is usually represented by the dimensionless quantity, $G\mu$, where G is the gravitational constant.

3.4 Types of defects

In general, the type of defect that is formed is defined by the nature of the symmetry breaking. Let us consider a general symmetry breaking:

$$G \to H\,, \tag{3.17}$$

where G is the group of transformations that leaves the Lagrangian density invariant and H is the subgroup of G which contains the transformations which leave the field invariant after it has developed a VEV; it is therefore called the unbroken subgroup. The vacuum manifold, $\mathcal{M}$, which represents the space of all equivalent vacua, can be identified with the coset

$$\mathcal{M} = G/H\,. \tag{3.18}$$

For example, in the case of the Goldstone model of a real scalar, Eqs. (3.8) and (3.9), the vacuum manifold was composed of the values $\pm\eta$. In the studied cases that formed cosmic strings, the vacuum manifold was the circle of minima of the "mexican hat" potential, Fig. 3.1. On the other hand, a monopole would be formed if the vacuum manifold was a sphere. In Fig. 3.5(a) a configuration which would lead to the formation of a monopole — a point like defect — is illustrated. This configuration is not continuously deformed to a vacuum solution — an example of a vacuum configuration is depicted in Fig. 3.5(b).

The type of defect that may be formed in a symmetry breaking is determined by the first homotopy group of the vacuum manifold, $\pi_n(\mathcal{M})$, which is non-trivial. Table 3.1 shows the relation between which homotopy group is non-trivial and the type of defect that is formed [1].

Table 3.1: Defect formed according to the non-trivial homotopy group of the vacuum manifold, $\mathcal{M}$

Homotopy Groups	**Defect to be formed**
$\pi_0 \neq 1$	Domain Walls
$\pi_1 \neq 1$	Cosmic Strings
$\pi_2 \neq 1$	Monopoles

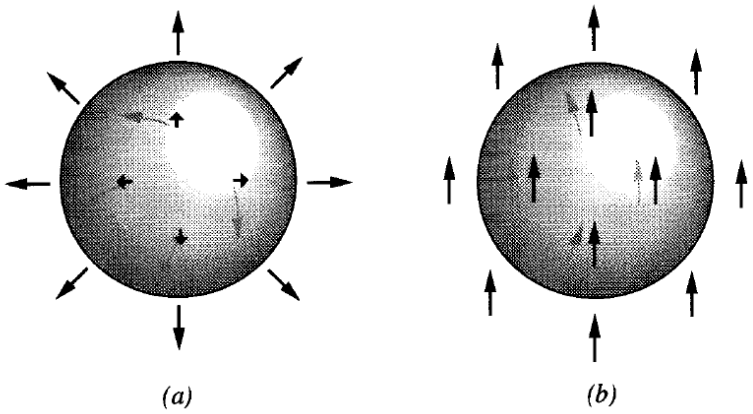

Figure 3.5: Left: Field configuration in 3 spatial dimensions which cannot be continuously deformed into a vacuum solution (right figure). This results in a point-like cosmological defect, a monopole [1].

Chapter 4

Cosmic String Network evolution

Cosmic strings may be formed when the first homotopy group of the vacuum manifold is non-trivial, $\pi_1(\mathcal{M}) \neq 1$. The circle of minima of the "mexican hat" potential, Fig. 3.1, was an example of such a cosmic string forming vacuum manifold. Cosmic strings are interesting objects of study for a couple of reasons: firstly, their length growth rate is expected to be faster than the expansion rate of the Universe throughout most of the cosmological history, resulting in structures of cosmological significance; moreover, they are expected — by numerical and semi-analytical models [21, 22, 23, 24, 25] — to evolve towards a regime of linear scaling both in the radiation and matter-dominated eras, which results in their energy density being a constant fraction of the energy density of the Universe. This implies that, unlike domain walls or monopoles, cosmic string networks are not predicted to dominate the energy density of the Universe [4].

One of the reasons that results in cosmic strings not dominating the energy density of the Universe is that the network loses energy. As strings interact, they may form closed loops which, under the effect of their tension oscillate, decaying through the emission of gravitational radiation. Therefore, cosmic string networks are expected to produce a stochastic gravitational wave background (SGWB) since they emit GWs throughout the cosmological history. The detection of gravitational waves in 2015 by the LIGO collaboration [5] has reignited interest in these defects and in the gravitational signature they produce.

But before estimating the SGWB spectrum generated by cosmic strings, let us study the dynamics of their evolution.

4.1 Velocity-dependent One Scale Model

Initial attempts at modelling the evolution of a string network [26, 27] were based on the one-scale assumption, which means that a single scale, the characteristic length of the string network, is enough to describe the entire dynamics of the network. Despite the successes of these models at describing the large-scale dynamics of the string network evolution — including the predicted linear scaling regime — they proved inadequate at small-scales. Models with more than one lengthscale were developed, including Refs. [28, 29]. However, despite the added complexity, these models did not provide a significant better insight into the dynamics of cosmic string networks.

In this work, the Velocity-dependent One Scale (VOS) model is used [24, 25]. This is a one-scale model but it was improved to consider the average root mean squared velocity of the network as a dynamical variable. Despite its simplicity, it has been shown to provide an accurate modelling of the large scale evolution of cosmic string networks [30, 31], while containing enough freedom to allow for a parameterization of various dynamical uncertainties and degrees of freedom. It provides a quantitative description of the network throughout its evolution, from the friction-dominated early evolution to the linear scaling regime.

To derive the VOS model, the string is considered a one spatial dimensional object, given that its length is generally much larger than its thickness. The world-history of a string can then be defined by a two-dimensional surface, the worldsheet, where

$$x^\sigma = x^\sigma(u^a)\,, \tag{4.1}$$

where $a = 0, 1$, $u^0(u^1)$ are the timelike (spacelike) coordinates that parameterize the worldsheet and x^σ are spacetime coordinates. An infinitely thin string obeys the Nambu-Goto action,

$$S = -\mu \int d^2u \sqrt{-\tilde{g}}\,, \tag{4.2}$$

where $\tilde{g}$ is the determinant of the induced metric, $\tilde{g}_{ab} = g_{\sigma\nu} x^\sigma_{,a} x^\nu_{,b}$, and $g_{\sigma\nu}$ is the metric of the background. Consider a flat Universe described by the FRW metric, with the line element

given by

$$ds^2 = a^2(\tau)(d^2\tau - d\mathbf{x}\cdot d\mathbf{x})\,, \tag{4.3}$$

where a is the scale factor, τ is the conformal time and $\mathbf{x}$ a 3-vector with comoving coordinates. The action given by Eq. (4.2) is invariant under reparameterizations of the worldsheet. Therefore, one may choose such a parameterization in which

$$\begin{aligned} u^0 &= \tau\,, \\ \frac{\partial \mathbf{x}}{\partial \tau}\cdot\frac{\partial \mathbf{x}}{\partial u^1} &= 0\,. \end{aligned} \tag{4.4}$$

The first condition identifies the worldsheet time with conformal time and the second one imposes that string velocity is orthogonal to the string direction[1]. These are called the temporal-transversed gauge conditions. From the Nambu-Goto action, Eq. (4.2), the energy of the string can be calculated:

$$E = \int d^3x\sqrt{-g}T^{00} = \int d^3x\sqrt{-g}\left(\frac{-2}{\sqrt{-g}}\frac{\delta S}{\delta g_{00}}\right) = \mu a(\eta)\int \epsilon du^1\,, \tag{4.5}$$

where

$$\epsilon = \left(\frac{\mathbf{x}'^2}{1-\dot{\mathbf{x}}^2}\right), \tag{4.6}$$

where dots and primes represent a derivative with respect to conformal time and to the spacelike parameter of the worldsheet, u^1, respectively.

Varying the Nambu-Goto action, Eq. (4.2), with respect to x^σ and taking into consideration the temporal-transverse gauge conditions, the string equations of motion can be written as [25]

$$\ddot{\mathbf{x}} + 2H(1-\dot{\mathbf{x}}^2)\dot{\mathbf{x}} = \frac{1}{\epsilon}\left(\frac{\mathbf{x}'}{\epsilon}\right)', \tag{4.7}$$

$$\dot{\epsilon} + 2H\dot{\mathbf{x}}^2\epsilon = 0\,, \tag{4.8}$$

where H is the Hubble parameter. The root-mean-square velocity of the network — which in

[1]This condition is a consequence of considering the string to be a 1-dimensional object.

the case of the VOS model is treated as dynamical variable — is defined as

$$\bar{v}^2 \equiv \langle \dot{\mathbf{x}}^2 \rangle = \frac{\int \dot{\mathbf{x}}^2 \epsilon du}{\int \epsilon du} \,. \tag{4.9}$$

Differentiating Eq. (4.5), one arrives at an equation for the evolution of the total energy density, $\rho \propto Ea^{-3}$, with respect to physical time,

$$\frac{d\rho}{dt} + 2H\rho(1+\bar{v}^2) = 0 \,. \tag{4.10}$$

However, in deriving Eq. (4.10), the energy loss by loop production was not considered. Let us introduce this energy loss by identifying two constituents of the string network: long strings and smaller closed loops. The large scale properties of long strings are studied under the assumption that a single lengthscale — the characteristic length L — is enough to characterize them. The characteristic lengthscale is defined as

$$\rho_\infty = \frac{\mu}{L^2} \,, \tag{4.11}$$

where ρ_∞ is the energy density of long strings.

The interaction of two strings or self-interactions may result in the formation of closed loops that detach from the long string network. Fig. 4.1 schematizes some possible outcomes of string interaction. These closed loops will oscillate under the effect of their tension and decay radiatively through the emission of gravitational waves. Therefore, the energy density that goes into these closed loops is eventually lost by the network. The rate of energy lost to the production of loops can be written as [2]

$$\left.\frac{d\rho_\infty}{dt}\right|_{loops} = \frac{\tilde{c}\bar{v}\rho_\infty}{L} \,, \tag{4.12}$$

where $\tilde{c}$ is a phenomenological parameter that quantifies the efficiency of the loop creation process. The value of $\tilde{c} = 0.23 \pm 0.04$ has been shown to provide a good fit to both radiation and matter eras cosmic string network simulations [24].

Another important aspect of string evolution is still missing. String motion is retarded by

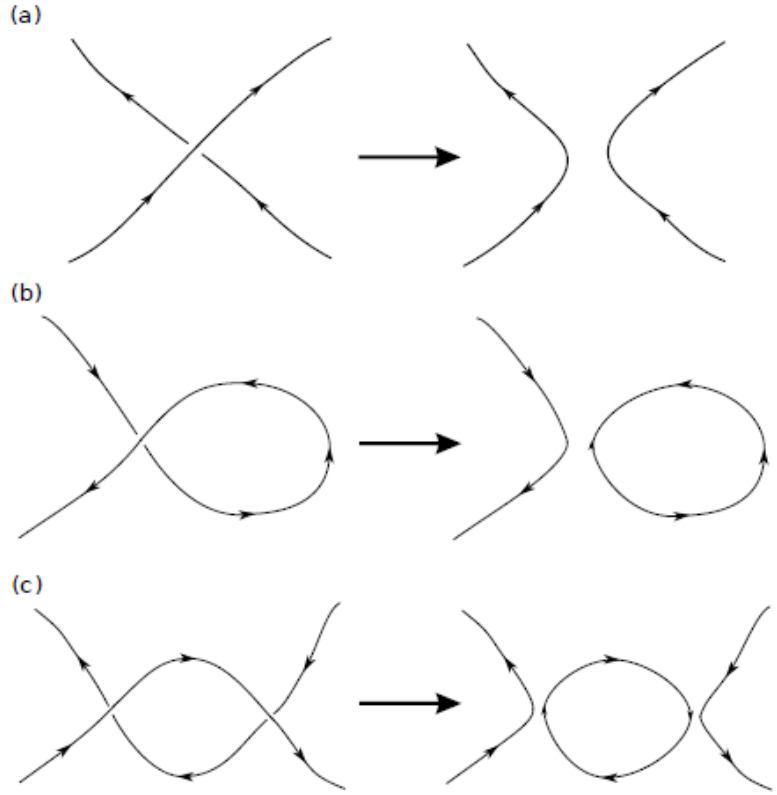

Figure 4.1: Possible results of string interaction. Top: Formation of two kinky strings. Middle: Self-interaction resulting in a closed loop. Bottom: Interaction between two strings resulting in a closed loop [32].

interactions with other cosmological components. The friction lengthscale, ℓ_f, which quantifies this effect, is given by [1]

$$\ell_f = \frac{\mu}{\sigma T^3}\,, \tag{4.13}$$

where T is the background temperature and σ is a numerical factor which takes into consideration the number of particle species interacting with the string. A damping lengthscale can also be defined, ℓ_d, which takes into consideration the damping caused by the expansion of the Universe and the friction effects, $\ell_d^{-1} = 2H + \ell_f^{-1}$.

Therefore, including loop production and friction effects in Eq. (4.10), the overall equation

for the evolution of the characteristic length of the string network can be obtained:

$$2\frac{dL}{dt} = \left(2H + \frac{\bar{v}^2}{\ell_d}\right)L + \tilde{c}\bar{v}\,. \tag{4.14}$$

The time evolution of $\bar{v}$ is calculated by differentiating Eq. (4.9),

$$\frac{d\bar{v}}{dt} = (1-\bar{v}^2)\left(\frac{k}{L} - \frac{\bar{v}}{\ell_f}\right), \tag{4.15}$$

where k is a dimensionless curvature parameter. It is a phenomenological parameter; however, in Ref. [24] a semi-analytical description of k was developed, as a function of $\bar{v}$,

$$k(\bar{v}) = \frac{2\sqrt{2}}{\pi}(1-\bar{v}^2)(1+2\sqrt{2}\bar{v}^3)\frac{1-8\bar{v}^6}{1+8\bar{v}^6}\,. \tag{4.16}$$

4.2 Evolution of Cosmic String Networks

Upon formation, a string network experiences a significant frictional damping from the relatively high radiation background density: it is thus important to study this friction dominated regime. Let us consider that, for the local cosmic strings forming model we studied in section 3.3 [1]

$$G\mu \sim \left(\frac{T_c}{m_{pl}}\right)^2, \tag{4.17}$$

where $\mu \sim \eta^2 \sim T_c^2$, where T_c is the critical temperature. Given that we are working on natural units, the Planck mass is given by $m_{pl} = t_{pl}^{-1} = G^{-1/2}$ allowing one to write Eq. (4.17). From Eq. (4.13), one can write the evolution of ℓ_f as

$$\ell_f \sim \frac{g^{1/2}}{\sigma}(tt_{pl})^{1/2}\left(\frac{T_c}{T}\right)^2, \tag{4.18}$$

where $g = 4\pi(\pi\mathcal{N}/45)^{1/2}$ and $\mathcal{N}$ is the number of relativistic degrees of freedom. To arrive at Eq. (4.18), the Friedmann equation was used, $H^2 = 8\pi G\rho/3$ — considering that the string network is created during the radiation dominated era, $H = (2t)^{-1}$ — and $\rho = \pi^2\mathcal{N}T^4/30$.

To understand whether friction effects are important, one must look at the damping length,

$\ell_d^{-1} = 2H + \ell_f^{-1}$, and see if the frictional effect is negligible when compared with the expansion of the Universe. At the time of creation, from Eq. (4.18) and considering that σ and g are of the order of unity:

$$\ell_f(t_c)H(t_c) \sim \frac{g^{1/2}}{\sigma}\left(\frac{t_{pl}}{t_c}\right)^{1/2} . \tag{4.19}$$

Therefore, $\ell_f H \ll 1$ at the time of creation of the string network if $t_c \gg t_{pl}$. Consequently, the initial evolution of the string network is friction dominated.

However, this regime is transient. The condition, $2H \gg \frac{\sigma T^3}{\mu}$, allows us to write when friction becomes negligible:

$$T \ll G\mu m_{pl} \, , \tag{4.20}$$

where numerical factors of order unity were ignored. After this moment, the evolution of the network can be considered frictionless and the VOS equations become:

$$\frac{dL}{dt} = LH + LH\bar{v}^2 + \frac{\tilde{c}\bar{v}}{2} \, , \tag{4.21}$$

$$\frac{d\bar{v}}{dt} = (1-\bar{v}^2)\left(\frac{k}{L} - 2\bar{v}H\right) . \tag{4.22}$$

Since loop production is expected to be suppressed during the friction dominated regime, throughout this work we will consider the network only starts producing loops at time t_i already in the frictionless regime ($\ell_f = \infty$), unless explicitly stated otherwise. This time is approximately given by

$$t_i \sim (G\mu)^{-1} t_f \, , \tag{4.23}$$

where t_f is the time of the string network formation.

4.2.1 The scaling regime

As expected from numerical simulations, [21, 22, 23, 24, 25], the VOS equations, Eqs. (4.21) and (4.22), have an attractor solution which corresponds to the linear scaling regime. In this regime, $\bar{v}$ is a constant and the characteristic length is proportional to physical time, $L = \xi t$, where ξ is a constant. The quantity LH, which will be of interest later, also becomes constant

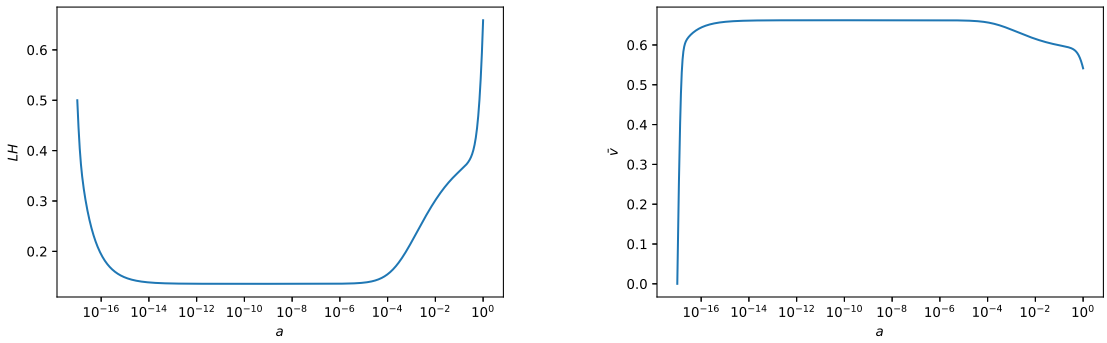

(a) (b)

Figure 4.2: Evolution of the quantity LH (a) and $\bar{v}$ (b) with the scale factor. Both quantities attain the scaling constant value in the radiation era, $(LH)_r \approx 0.136$ and $\bar{v}_r \approx 0.662$. However, in this case which was calculated with $\tilde{c} = 0.23$, the matter era is not long enough for the network to attain the scaling regime.

in the scaling regime, $LH = \xi\beta$ — valid deep in the matter or radiation dominated eras where $H = \beta/t$.

This regime is important because, if the network is in linear scaling, the string energy density becomes a constant fraction of the energy density of the Universe, during both the radiation and matter eras:

$$\frac{\rho_\infty}{\rho_r} \propto \frac{\mu/(\xi_r t)^2}{a^{-4}} = \mu/\xi_r^2 \quad \text{and} \quad \frac{\rho_\infty}{\rho_m} \propto \frac{\mu/(\xi_m t)^2}{a^{-3}} = \mu/\xi_m^2 \,. \tag{4.24}$$

where $a \propto t^\beta$ was used with $\beta = 1/2$ for the radiation epoch and $\beta = 2/3$ for the matter dominated era. Notice that ξ and $\bar{v}$ take different values in the scaling regime in the radiation dominated era, $\bar{v}_r$ and ξ_r, and in the matter dominated one, $\bar{v}_m$ and ξ_m. Cosmic strings are therefore not predicted to dominate the energy density of the Universe at later times [33].

It must be noted that this regime is only attainable deep into the radiation or matter eras. This can be seen in Figs. 4.2a and 4.2b, which show the evolution of LH and $\bar{v}$ with the scale factor, a, for a network with initial conditions different from the scaling regime. In the radiation era, both quantities evolve towards a constant value. However, during the radiation-matter transition ($a_{eq} \sim 10^{-4}$) , the scaling regime is not valid. Furthermore, as the Universe evolves to a Λ dominated era, the matter epoch might not be long enough for the network to reattain this regime.

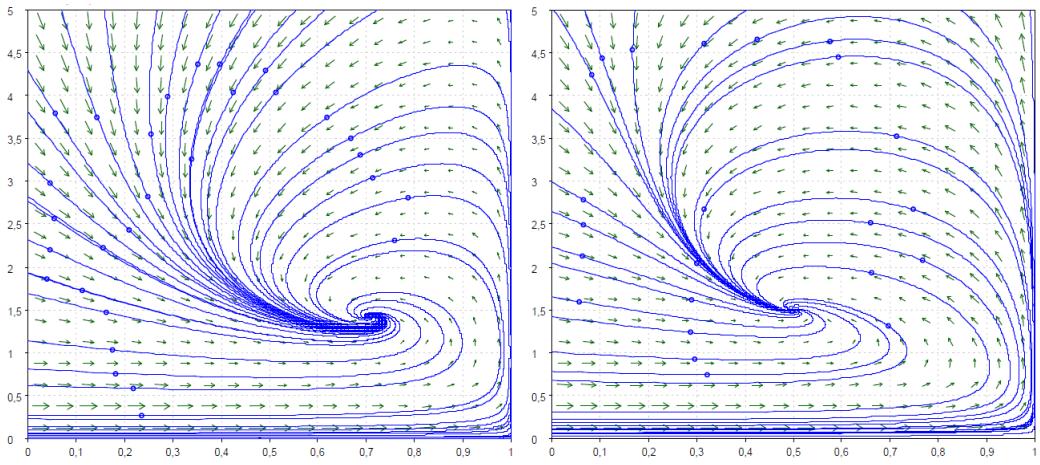

(a) (b)

Figure 4.3: Phase portrait illustrating the evolution of $\bar{v}$ (in the horizontal axis) and of ξ (in the vertical axis) in a radiation dominated era (a) and a matter dominated era (b). In both cases, $\tilde{c} = 1$ and $k = 1$ were used. The blue lines represent trajectories of the variables following the differential Eq. (4.25). Each line represents a different initial condition. Every case evolves towards a fixed point, corresponding to the value calculated in Eq. (4.26)

The scaling values of $\bar{v}$ and ξ can be calculated by substituting the characteristic length by $L = \xi(t)t$ — where, for now, ξ is assumed to be a function of time — and $H = \beta/t$, resulting in

$$\frac{d\xi}{dt} = \frac{\xi\beta(1+\bar{v}^2) + \frac{\tilde{c}\bar{v}}{2} - \xi}{t} \quad \text{and} \quad \frac{d\bar{v}}{dt} = \frac{(1-\bar{v}^2)\left(\frac{k}{\xi} - 2\bar{v}\beta\right)}{t}. \tag{4.25}$$

The linear scaling regime is expected to be a fixed point of the system of differential Eqs. (4.25). Therefore, setting $d\bar{v}/dt = 0$ and $d\xi/dt = 0$ to check for fixed points, one gets:

$$\xi = \sqrt{\frac{k(k+\tilde{c})}{4\beta(1-\beta)}} \quad \text{and} \quad \bar{v} = \sqrt{\frac{k}{k+\tilde{c}}\frac{1-\beta}{\beta}}. \tag{4.26}$$

Fig. 4.3 shows that these solutions are global attractors of the VOS equations by illustrating the evolution of the variables in a phase portrait. In this phase portrait, the time variable was set to $t' = \ln(t)$. Every trajectory (corresponding to different initial conditions) evolves towards the fixed point which corresponds to the values of Eq. (4.26). Thus, in a frictionless regime, every network will eventually reach the scaling regime if it spends enough time in the radiation or matter dominated eras.

4.2.2 Stretching regime

Another important regime takes place when the initial characteristic length of the network is sufficiently large, $LH \gg \frac{\tilde{c}\bar{v}}{2}$. In this case, it can be shown that the network evolves according to [34]

$$L \propto a \quad \text{and} \quad \bar{v} \propto (aH)^{-1} \propto a^{-1-1/\beta} \to 0\,. \tag{4.27}$$

Figs. 4.4a, 4.4b and 4.4c depict the cosmological evolution of L/a, LH and $\bar{v}$ respectively, for networks with an initial characteristic length sufficiently large to enter the stretching regime. In each of these figures, a standard case — here standard corresponds to a network with initial conditions set to the values of the scaling regime in the radiation era — is also depicted for comparison. The first condition of Eq. (4.27) can observed in Fig. 4.4a, as L/a remains a constant while the network is in the stretching regime.

From these figures, one can observe that the stretching regime is transient and the network eventually evolves towards the scaling regime, despite it suffering a significant delay. A larger initial LH implies that the network enters the scaling regime at a later time. In Fig. 4.4c the second condition for $\bar{v}$ in Eq. (4.27) is observed, with $\bar{v}$ taking a value very close to 0 while in the stretching regime. From Eq. (4.12), this implies that loop production is significantly suppressed. If loops are assumed to be the main sources of GWs by the network, one can say that GW emission is supressed during the stretching regime.

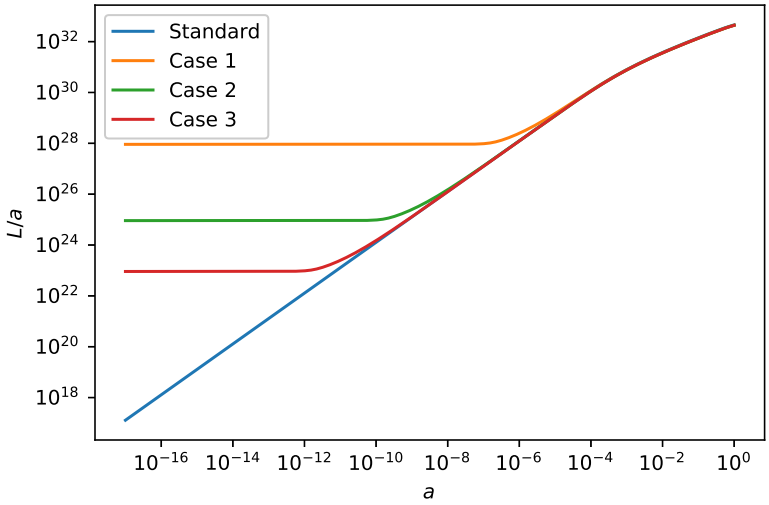

(a)

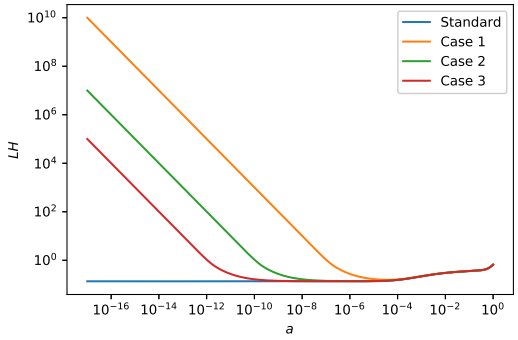

(b)

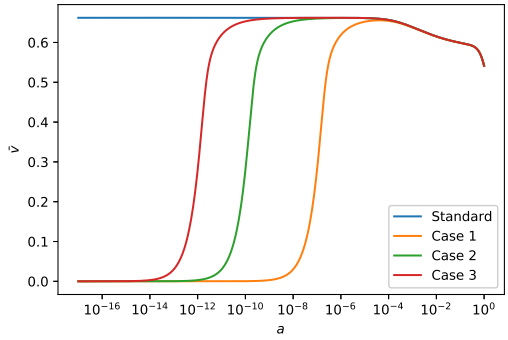

(c)

Figure 4.4: Cosmological evolution of L/a (a), LH (b) and $\bar{v}$ (c) for cases with different initial conditions for LH, $(LH)_1 > (LH)_2 > (LH)_3 \gg 1$. In blue the evolution for a standard network is illustrated for comparison — standard corresponds to a network with initial onditions set to the values of the scaling regime. The loop-chopping efficiency was set to $\tilde{c} = 0.23$.

Chapter 5

Computation of the SGWB Spectrum

The mechanism through which a network of cosmic strings emits gravitational waves (GWs) must be studied to compute the stochastic gravitational wave background (SGWB) spectrum.

The main contribution to the SGWB spectrum produced by a network of cosmic strings is generally expected to come from the emission of GWs resulting from the oscillation of closed loops. These loops are created due to interactions between different cosmic strings (or self-interactions) and detach from the long string network. Imposing periodic boundary conditions to the equations of motion derived from the Nambu-Goto action, the period of these oscillations is calculated to be $T = l/2$ [1], where l is the characteristic length of the loops. This length is defined as $E_l = \mu l$, where E_l is the energy of the loop.

Given that $f = T^{-1}$, the frequency f_j of gravitational waves emitted by cosmic loops is expected to be:

$$f_j = \frac{2j}{l}\,, \tag{5.1}$$

where $j = 1, 2, \cdots$ is the harmonic mode of emission and f_j its corresponding frequency.

From the definition of $l = E_l/\mu$, one may conclude that, as the loop radiates gravitational waves and loses energy, its characteristic length decreases from the time of its formation until it completely decays and disappears. Therefore, from Eq. (5.1), it follows that a loop will emit GWs on a wide range of frequencies due to the frequency's dependence on $l(t)$. In fact, a loop

is expected to emit GWs with frequencies going from f_{min} to ∞, where $f_{min} = 2/l_b$ represents the minimum frequency of the GWs radiated by a loop and l_b is its characteristic length upon its birth.

It is important to note that the mentioned frequency represents the frequency with which the gravitational wave is emitted. As seen previously, as it travels through space, a gravitational wave suffers a redshift in frequency as a result of the background expansion which increases its wavelength. Therefore, gravitational waves which were emitted with frequency f_{em} are observed today with a smaller frequency f_{obs}. In fact, using Eq. (2.4) where the redshift of frequencies was introduced, one can write the observed frequency as

$$f_{j_{obs}} = \frac{2j}{l(t)} \frac{a(t)}{a_0} \,, \tag{5.2}$$

where a_0 is the scale factor today, which will be taken to be $a_0 = 1$ throughout this work; the subscript 0 will be used to refer to the value that variables take at the present time. The instant t considered is the time of emission of the GW.

To estimate in which frequency a loop is emitting at a specific time t, one needs to know how the characteristic length evolves. From the quadrupole formula the gravitational radiation power can be estimated to be [1]

$$\frac{dE}{dt} \sim GM^2 l^4 f^6 \,, \tag{5.3}$$

where, considering $M = \mu l$ and $f \propto l^{-1}$,

$$\frac{dE}{dt} = \Gamma G \mu^2 \,. \tag{5.4}$$

Here Γ is a constant parameter which describes the efficiency of the gravitational wave emission mechanism, which we will take to be $\Gamma \sim 65$ according to [7, 35]. From Eq. (5.4) one can conclude that loops lose energy through gravitational radiation at a roughly constant rate. From the definition of characteristic length of the loop, one arrives at $dl/dt = -\Gamma G\mu$ — the minus sign comes from the fact that the loops lose this energy. Therefore the loop evolution can be written as

$$l(t) = l_b - \Gamma G \mu (t - t_b) \,, \tag{5.5}$$

which is valid for $t_b < t < t_d$, where the subscripts b and d indicate that the value of the variable is being taken at the time of birth or death of the loop, respectively.

Numerical simulations have been inconclusive regarding the size with which loops are formed after interactions of long strings, l_b. While some simulations have shown that a significant part of the energy lost by the netork goes into the formation of large loops, others have found no evidence of a population of large loops [36].

Given this uncertainty, we shall take an alternative approach — introduced in [37] and later extended [33, 38] — in which the size of the loops is treated as a free parameter and one has enough plasticity to probe a large variety of cosmic string scenarios. Let us then assume that loops are created with a size that is a fixed fraction of the characteristic length of the network at the time of birth, t_b, so that

$$l_b = \alpha L(t_b)\,, \tag{5.6}$$

where α is a constant parameter. Although one does not realistically expect all loops to be created with exactly the same size — instead the distribution of the sizes of loops formed at the time t_b is expected to peak around l_b — if the width of the distribution is not very large, this should be a good approximation (see Ref. [38] for a discussion on the effect of this assumption).

From Eq. (5.5), one can estimate the life-time of a loop, $\Delta t = t_d - t_b$, by setting $l(t_d) = 0$,

$$\Delta t = \frac{\alpha L(t_b)}{\Gamma G \mu}\,. \tag{5.7}$$

Since they eventually decay, cosmic string loops are thus predicted to generate a transient gravitational wave signal. However, due to the existence of several loops at any given time in cosmic history, the superimposition of the bursts of GWs they emit is expected to give rise to a Stochastic Gravitational Wave Background (SGWB) [7, 9, 39]. The amplitude of SGWB generated by cosmic string networks is often quantified using the energy density of GW, $\rho_{\rm GW}$, per logarithmic frequency interval (in units of the critical density $\rho_{\rm c}$),

$$\Omega_{GW} = \frac{1}{\rho_c}\frac{d\rho_{GW}}{d\log f}\,. \tag{5.8}$$

To find the spectral energy density in GW at the present time, one must consider contributions

from GWs emitted by loops created from the time of formation of the network until today which, after suffering the specific redshfit, have a frequency f at the present time.

The contribution from all modes of emission can be taken into account in the spectral density through a weighted sum:

$$\Omega_{\rm GW}(f) = \sum_{j}^{n_s} \frac{j^{-q}}{\mathcal{E}} \Omega^{j}_{\rm GW}(f)\,, \tag{5.9}$$

where

$$\mathcal{E} = \sum_{m}^{n_s} m^{-q}\,, \tag{5.10}$$

n_s is the number of harmonic modes that have been taken into consideration and q is a parameter that depends on the shape of the loops. It has been shown that $q = 2$ for loops with kinks, while $q = 4/3$ for loops with cusps [39]. Previous work [38] has shown that, in general, it is sufficient to consider modes up to $n_s = 10^3$ or $n_s = 10^5$ for loops with a kink or a cusp, respectively. In fact, for these values, the SGWB reaches a "saturation" and remains essentially unchanged by the inclusion of any higher order terms. For the remainder of this work, we shall restrict ourselves to the fundamental mode of emission. However, note that, since

$$\Omega^{j}_{\rm GW}(jf) = \Omega^{1}_{\rm GW}(f)\,, \tag{5.11}$$

one may easily construct $\Omega^{j}_{\rm GW}$ for any arbitrary mode of emission j, once the spectrum associated to the fundamental mode is computed.

In the small-loop regime, some assumptions simplify the computation of the SGWB spectrum. Therefore, we will start by studying this regime.

5.1 The small-loop regime

The small-loop regime is characterized by loops with a length $l \ll \Gamma G\mu t$ and this fact has important consequences on their life-time [40]. One should note that this definition also applies to loops that are created large but which, as time goes by, enter the small-loop regime (as their length decreases). However, in this section, we will only consider loops that are created small,

and therefore the definition can be further specified to $\alpha \ll \Gamma G\mu$.

From Eq. (5.7), and considering the scaling regime $L = \xi t$, one can conclude that small loops are expected to live significantly less than a Hubble time, $t_H = H^{-1}$. Consequently, one can assume that these loops decay instantly and their energy is radiated in GWs immediatly after their formation. Note, however, that the energy of small loops is not radiated in a single frequency, since the frequency of GWs is expected to increase as the length decreases. The range of frequencies is still $f_{min} < f < \infty$. The importance of the assumption of instant decay is that, since all the energy is radiated roughly at the same moment in time, every frequency of waves emitted by the same loop suffers the same redshift. This simplifies the calculation of the SGWB spectrum.

One can calculate the distribution of energy over the different frequencies by using the following probability distribution function [40]

$$p(f) = \frac{dE}{df}\frac{1}{E_{0l}} = \mu\frac{dl}{df}\frac{1}{\mu l_b}\,, \tag{5.12}$$

where E_{0l} is the energy of the loop at the time of formation. From $dl/df = -2a(t_b)/f^2 a_0$, $p(f)$ becomes, for small loops,

$$p(f) = \frac{f_{min}}{f^2}\Theta(f - f_{min})\,, \tag{5.13}$$

where $\Theta(f - f_{min}) = 1$ for $f > f_{min}$ and vanishes for all other f.

From Eq. (5.13), the way a loop distributes its energy over frequencies is known. Moreover, from the VOS model and Eq. (4.12), one can estimate the energy density the network loses to the creation of loops in each instant. Hence, one can write,

$$\left.\frac{d\rho_{GW}}{df dt}\right|_{loops} = \frac{\tilde{c}\bar{v}\mu}{L^3}\left(\frac{a(t)}{a_0}\right)^4\frac{f_{min}}{f^2}\Theta(f - f_{min})\,, \tag{5.14}$$

where the term dependent on the scale factor represents the dilution of the energy density of radiation by the background expansion.

To arrive at the SGWB spectrum defined by Eq. (5.8), Eq. (5.14) has to be integrated:

$$\Omega_{GW}(f) = \frac{16\pi G}{3H_0^2}\frac{\tilde{c}\mu}{a_0^5}\frac{1}{\alpha f}\int_{t_{min}}^{t_0}\frac{\bar{v}(t)}{L^4(t)}a^5(t)dt\,, \tag{5.15}$$

where the lower bound of the integral t_{min} is the time of creation of loops for which $f_{min} = f$, where f is the frequency point for which the spectrum is being calculated. Note that, if $t_{\min} \leq t_i$, where t_i is the time when the creation of loops is assumed to start, the lower bound of the integral is simply t_i, losing its dependence on f.

To understand which loops contribute most to which range of frequencies, some aspects must be taken into account:

- from Eq. (4.12), it follows that the energy density that goes into the formation of loops decreases with time;
- the same happens for f_{min}, defined as

$$f_{min} = \frac{2}{\alpha L(t)} \frac{a(t)}{a_0}\,, \tag{5.16}$$

  which decreases monotonically throughout cosmological history;
- furthermore, the probability distribution given by Eq. (5.13) shows that loops emit most of their energy density in GWs with frequencies near f_{min}.

Therefore, it is possible to conclude that the main contributors to the high frequency range of the SGWB spectrum are the smallest loops formed, created in the radiation era, while in the low frequency range, the main contribution comes from loops created during the matter era.

The following spectrum (and all other presented SGWB spectra) was computed by an algorithm developed during this thesis. Fig. 5.1 shows the SGWB spectrum, calculated following Eq. (5.15), for a network with $\alpha = 10^{-10}$ and $G\mu = 10^{-7}$. This figure illustrates the typical shape of the spectrum produced by a network of cosmic strings created in the small-loop regime. A constant plateau can be observed for higher frequencies caused by loops created in the radiation era, while a peak appears for lower frequencies, produced by loops formed in the matter era. The decrease in Ω_{GW} for frequencies lower than the position of the peak is a result of the natural cut-off we employ by setting the present time as the upper bound of integration in Eq. (5.15).

By assuming a scaling regime deep in the radiation era, the constant value of the high frequency range can be calculated analitically. The value of the spectrum at high frequencies,

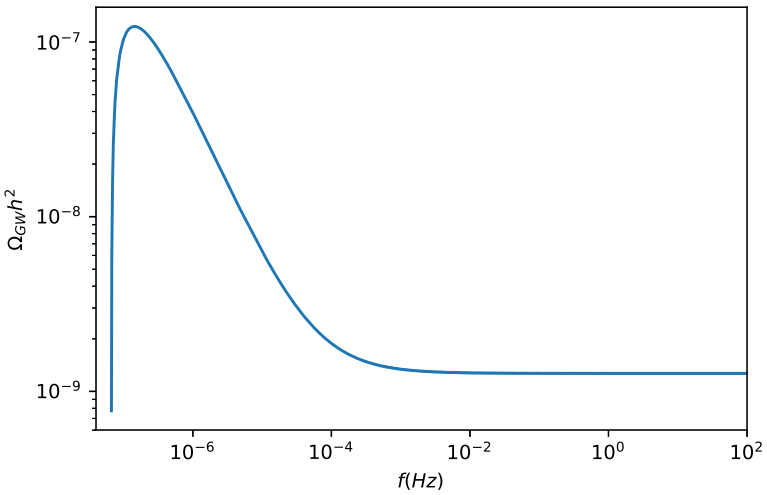

Figure 5.1: The SGWB spectrum produced by a network of cosmic strings, calculated following Eq. (5.15). This network is in the small-loop regime with $\alpha = 10^{-10}$ and $G\mu = 10^{-7}$. The loop-chopping efficiency is set to $\tilde{c} = 0.23$.

Ω_{GW_r}, can be calculated as

$$\Omega_{GW_r} = \frac{16\pi G}{3H_0^2}\frac{\tilde{c}\bar{v}_r\mu}{a_0^5}\frac{1}{\alpha f}\frac{1}{\xi_r^4}\int_{t_{min}}^{t_{eq}}\left(\frac{a(t)}{a(t_{eq})}\right)^5\frac{a^5(t_{eq})}{t^4}dt\,, \tag{5.17}$$

where the subscript r means that the scaling constants take the values in the radiation era. The instant t_{eq} denotes the moment when the radiation and matter energy densities are equal. Since only loops created in the radiation era are important to the high frequency range of the spectrum, one does not need to integrate until the present time to calculate the value of the plateau. The integral can be calculated as

$$\int_{t_{min}}^{t_{eq}}\left(\frac{t}{t_{eq}}\right)^{5/2}t^{-4}a^5(t_{eq})dt = -\frac{2a^5(t_{eq})}{t_{eq}^{5/2}}\left(t_{eq}^{-1/2} - \frac{f\xi_r\alpha t_{eq}^{1/2}a_0}{2a(t_{eq})}\right) \simeq f\xi_r\alpha\frac{a^4(t_{eq})a_0}{t_{eq}^2}\,, \tag{5.18}$$

where t_{min} was considered to be

$$t_{min} = \frac{2}{\alpha\xi\sqrt{t_{eq}}f}\frac{a(t_{eq})}{a_0}\,. \tag{5.19}$$

Substituting this result in Eq. (5.18), one gets the constant value

$$\Omega_{GW_r} = \frac{16\pi G}{3H_0^2}\frac{\tilde{c}\bar{v}_r\mu}{\xi_r^3}\left(\frac{a(t_{eq})}{a_0}\right)^4\frac{1}{t_{eq}^2}\,, \tag{5.20}$$

which coincides with the analytical result obtained in Ref. [40]. It is also possible to obtain the value of the flat part of the spectrum without the dependence on t_{eq}. To do so, considering that we are deep in the radiation era, the Hubble parameter as defined in Eq. (2.22) is dominated by the term relative to the energy density of radiation observed today, $\Omega_{0,r}$, and therefore the value of the plateau can be rewritten as

$$\Omega_{GW_r} = \frac{8\pi G\mu}{3}\frac{\tilde{c}\bar{v}_r}{(LH)_r^3}\Omega_{0,r}\,, \tag{5.21}$$

taking into consideration that LH is also a constant quantity in the scaling regime.

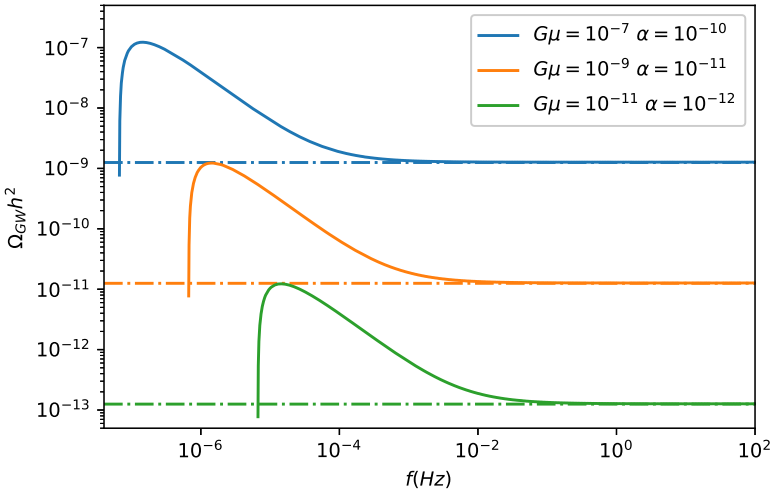

Figure 5.2: SGWB spectra produced by a network of cosmic strings, for different cases in the small-loop regime. The dash-dotted lines represent the plateau calculated analytically, following Eq. (5.21). The loop-chopping efficiency is set to $\tilde{c} = 0.23$.

In Fig. 5.2, SGWB spectra are compared with the value obtained in Eq. (5.21) to prove that these values coincide with the flat part of the spectrum for different cases in the small-loop regime.

Another important signature of a typical SGWB spectrum occurs for very high frequencies.

As mentioned, for high enough frequencies for which $t_{min} < t_i$, the lower bound of the integral of Eq. (5.15) becomes t_i and the integral loses its dependence on f. Therefore one gets the behaviour of

$$\Omega_{GW} \propto f^{-1}\,, \tag{5.22}$$

which can be observed in Fig. 5.3, for very high frequencies, as a line of slope -1 (since the spectrum is represented in $\log - \log$ scale). For this very high range of frequencies (with $f \gg f_{\min}(t_i)$), the only contributions to the spectra will come from the end stages of the life of loops created throughout cosmological history. This is merely a consequence of the fact that the production of cosmic string loops has not been happening since the beginning of the universe, instead it is expected to start being significant at a time t_i. Therefore, there are no loops emitting dominantly at frequencies $f \gg f_{\min}(t_i)$. The smallest loops created by the network are the main contributors and, consequently, are responsible for this signature.

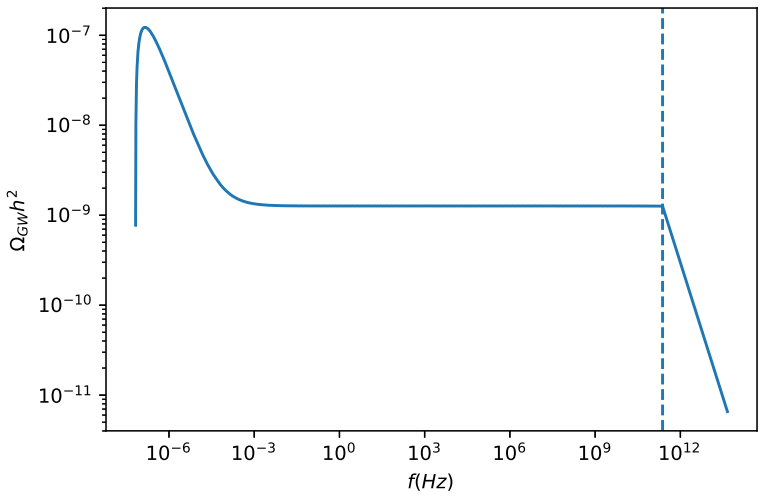

Figure 5.3: The SGWB spectrum produced by a network of cosmic strings with $\alpha = 10^{-10}$ and $G\mu = 10^{-7}$. The dashed line indicates the position of $f_{min}(t_i)$. For higher frequencies, the behaviour $\Omega_{GW} \propto f^{-1}$ is observed. The loop-chopping efficiency is set to $\tilde{c} = 0.23$.

5.1.1 Dependency on α

In the small-loop regime the shape of the SGWB spectrum is independent of the value of α. In fact, we have explicitly demonstrated that the flat part of the spectrum is independent

of the value of α in Eq. (5.21).

The effect of changing the value of α in the case of small loops is simply to shift the spectrum in the frequency axis, which is illustrated in Fig. 5.4, where the spectrum is represented for different values of α.

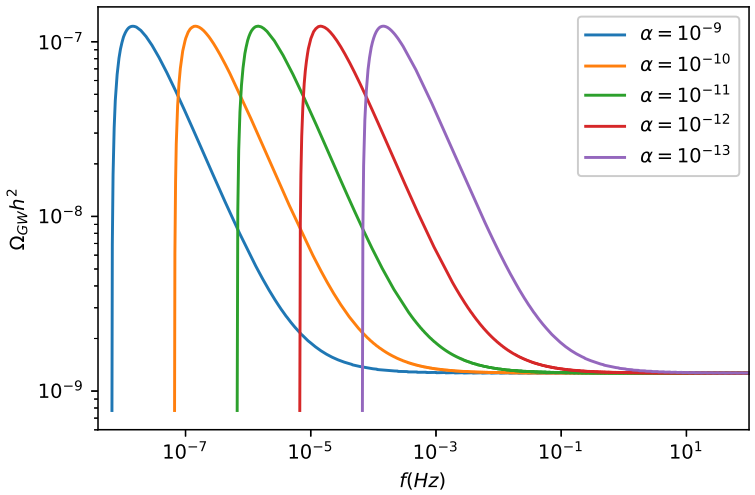

Figure 5.4: SGWB spectra produced by a network of cosmic strings with $G\mu = 10^{-7}$ for different values of α, all in the small-loop regime. The loop-chopping efficiency is set to $\tilde{c} = 0.23$.

5.1.2 Dependency on $G\mu$

The value of $G\mu$ affects the spectrum density both directly, as seen in Eq. (5.15), and indirectly since the life-time of a loop is affected by the value of $G\mu$. However, in the small-loop regime, since loops decay instantly, this indirect effect is not important. Therefore the amplitude of the spectrum changes proportionally to $G\mu$, $\Omega_{GW} \propto G\mu$, as can be observed in Fig. 5.5.

5.2 Large-loop regime

When loops are created large, $\alpha \gg \Gamma G\mu$, the assumption that they decay instantaneously is no longer valid. The computation of the SGWB spectrum is not as simple as in the case of small loops since the same loop emits GWs which suffer different redshifts. Recall, however,

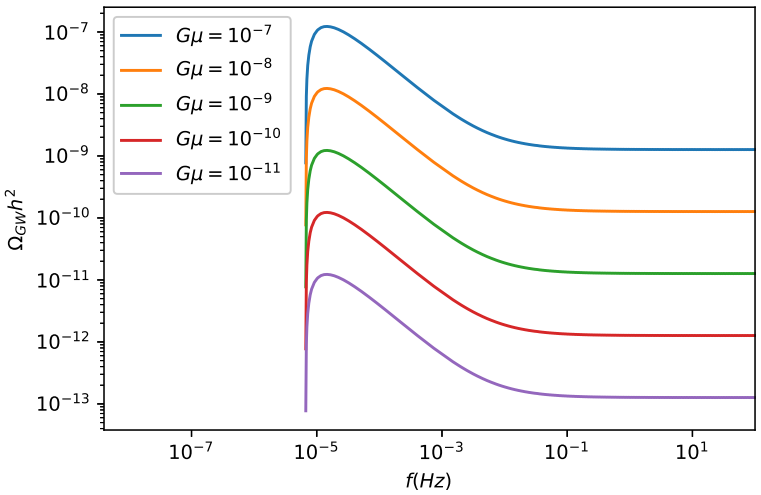

Figure 5.5: SGWB spectra produced by a network of cosmic strings with $\alpha = 10^{-12}$ for different values of $G\mu$, all in the small-loop regime. The loop-chopping efficiency is set to $\tilde{c} = 0.23$.

that large loops eventually enter the small-loop regime as their length decreases, decaying in less than a Hubble time from that moment on.

Let us start by calculating the way a loop distributes its energy by the frequencies of its emitted GWs:

$$\frac{dE}{df} = \mu \frac{2}{f^2} \frac{a_{em}}{a_0} \left(\frac{1}{1 + \frac{2H_{em}a_{em}}{\Gamma G \mu f a_0}} \right), \tag{5.23}$$

where a_{em} is the scale factor corresponding to the moment the gravitational wave with frequency f is emitted and H_{em} is the value of the Hubble parameter at this instant. The moment a loop emits GWs with frequency f, can be estimated as

$$\frac{a_{em}}{a_0} = \frac{f}{2}[\alpha L_b - \Gamma G \mu (t_{em} - t_b)]\,. \tag{5.24}$$

Note that we have calculated the distribution of energy by frequency for a single loop; therefore, we need to determine the number density of loops that are created at each moment by the network, n_c. This can be accomplished by dividing the energy density that goes into

the creation of loops by the energy of a single loop, resulting in

$$\frac{dn_c}{dt} = \frac{\tilde{c}\bar{v}}{\alpha L^4}\,. \tag{5.25}$$

Recall that it was assumed that all loops are created with the same physical length — and therefore energy — at each moment. With this in mind, the computation of the SGWB spectrum can be done following

$$\Omega_{GW}(f) = \frac{8\pi G}{3H_0^2}\int_{t_{min}}^{t_0} \frac{dn_c}{dt}\left(\frac{a(t)}{a_0}\right)^3 \frac{dE}{df}\frac{a_{em}}{a_0}dt\,. \tag{5.26}$$

Fig. 5.6 shows the SGWB spectrum calculated follwing Eq. (5.26) for $\alpha = 10^{-1}$ and $G\mu = 10^{-7}$, which is clearly in the regime of large loops. The discussion about the main contributions to the spectrum remains the same as in the small-loop regime: the flat part of the spectrum — higher frequencies — is a result of GWs emitted by loops created in the radiation era and the lower frequency range of the spectrum is a result of loops emitting GWs during the matter era. Note that, since we are in the large-loop regime, the loops which emit in the matter dominated era, may have been created earlier in the radiation epoch.

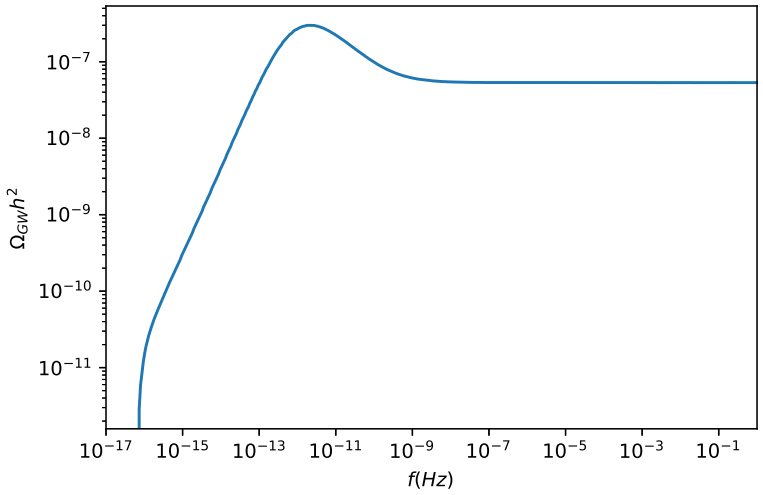

Figure 5.6: The SGWB spectrum produced by a network of cosmic strings, calculated following Eq. (5.26). This network is in the large-loop regime with $\alpha = 10^{-1}$ and $G\mu = 10^{-7}$. The loop-chopping efficiency is set to $\tilde{c} = 0.23$.

However, the analytical calculation of the flat part of the spectrum is not as immediate as before. Let us impose an artifical condition: a loop emits all of its energy at the time of its death, t_d. The redshift from the time of the death of the loop until the present time is given by

$$\frac{a_d}{a_0} = \frac{a_b}{a_0}\chi^\beta \,, \tag{5.27}$$

where

$$\chi = \left(\frac{\alpha\xi}{\Gamma G\mu} + 1\right). \tag{5.28}$$

The energy that is radiated by a loop, observed at the end of its life, E_{rd}, can be calculated using the equation of continuity of radiation energy density, Eq. (2.14), with the inclusion of a source: the loops which are continously emitting GWs. Therefore,

$$\frac{dE_r}{dt} + HE_r = \Gamma G\mu^2 \,, \tag{5.29}$$

where E_r represents the energy that has been radiated by a loop. Considering the condition that $E_r(t_b) = 0$, the radiation energy at the time of death of the loop becomes

$$E_{rd} = \frac{E_{0l}}{1+\beta} + \frac{\Gamma G\mu^2}{1+\beta}\left[t_b\left(1 - \frac{a_b}{a_d}\right)\right]. \tag{5.30}$$

For large loops, considering $a_d \gg a_b$ and $E_{0l} \gg \Gamma G\mu^2 t_b$, Eq. (5.30) becomes

$$E_{rd} \simeq \frac{E_{0l}}{1+\beta}\,. \tag{5.31}$$

For small loops, one can expand $\chi^\beta \simeq 1 + \frac{\beta E_{0l}}{\Gamma G\mu^2 t_b}$ resulting in

$$E_{rd} \simeq \frac{E_{0l}}{1+\beta} + \frac{\Gamma G\mu^2 t_b}{1+\beta}\frac{\beta E_{0l}}{\Gamma G\mu^2 t_b} \simeq E_{0l}\,, \tag{5.32}$$

which was expected considering that in the small-loop regime the loop decays instantaneously.

The analytical calculation of the flat part of the spectrum can be done using the distribution of energy of Eq. (5.23), but that is not necessary. In fact, to calculate the flat part of the spectrum, the distribution of energy is not important as long as the integral includes the main

contributors to the frequency range we are studying. The upper bound of the integral in Eq. (5.26) must be in the radiation era to perform analytical calculations and must be large enough to assure that the main contributions to the flat part of the spectrum are being considered. Therefore, for this analytical calculation, we will use the distribution of small loops since it has already been presented and it is normalized, Eq. (5.13), resulting in:

$$\Omega_{GW}(f) = \frac{8\pi G}{3H_0^2}\int_{a_{min}}^{\bar{a}} \frac{\tilde{c}\bar{v}}{\alpha(LH)^4} H^3 \left(\frac{a^2}{a_0^3}\right) \frac{E_{0l}}{1+\beta}\frac{a}{a_0}\chi^{\beta}\frac{f_{min}}{f^2}da\,, \tag{5.33}$$

where $\bar{a}$ is the scale factor corresponding to an instant deep in the radiation era and we are considering a range of frequencies high enough so that $a_{min} \ll \bar{a} \ll 1$. The Hubble parameter is used so we can consider LH (which is a constant quantity) and to change the variable of integration. The constant part of the spectrum can be calculated to be

$$\Omega_{GW_r} = \frac{8\pi G}{3}\frac{\tilde{c}\bar{v}_r\mu}{(LH)_r^3}\Omega_{0,r}\chi^{1/2}\left[2\alpha(LH)_r + \Gamma G\mu\left(1-\left(\frac{1}{\chi}\right)^{1/2}\right)\right]\frac{1}{3(LH)_r}\,, \tag{5.34}$$

where the Hubble parameter as defined in Eq. (2.22) is dominated by the term relative to the energy density of radiation observed today, $\Omega_{0,r}$.

In Fig. 5.7 some SGWB spectra calculated numerically are compared with the value obtained in Eq. (5.34) to assert that these values coincide with the flat part of the spectrum for different cases in the large loop regime.

We chose not to use the energy distribution by frequency of large loops, Eq. (5.23), to simplify the calculations of the value of the plateau. However this calculation can be performed in the radiation era, since there is a correspondence between the emission time and the frequency for each loop. Deep in the radiation era, from Eq. (5.24), one has

$$\frac{t_{em}^{1/2}}{t_d^{1/2}} = \frac{f}{2}[\alpha L_b - \Gamma G\mu(t_{em}-t_b)]\,, \tag{5.35}$$

which can be solved in terms of emission time as a function of f. We are considering that the observation is at the time of death of the loop, t_d.

Substituting this into the energy distribution, Eq. (5.23), one gets, considering that t_d is

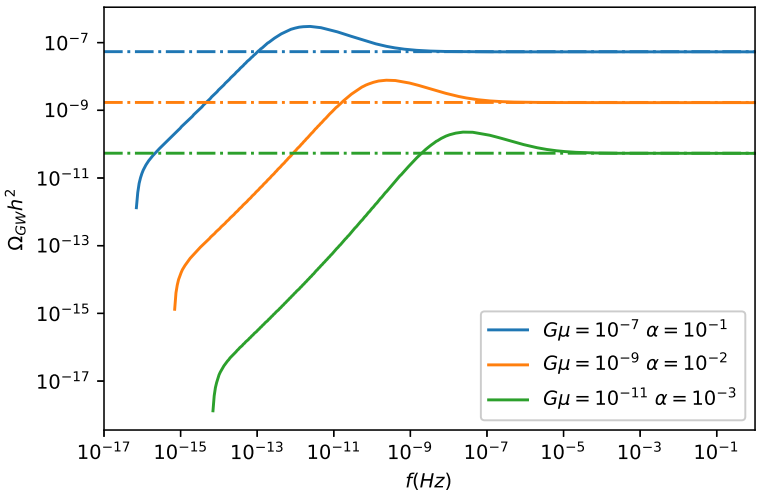

Figure 5.7: SGWB spectra produced by a network of cosmic strings, for different cases in the large-loop regime. The dash-dotted lines represent the plateau calculated analytically, following Eq. (5.34). The loop-chopping efficiency is set to $\tilde{c} = 0.23$.

the instant of observation,

$$\frac{dE}{df}\frac{a_{em}}{a_d} = \frac{4\mu^3}{E_{0l}^2}\left(\frac{1-\sqrt{1+l_b^2 f^2}}{f^4+\frac{f^4}{-1+\sqrt{1+l_b^2 f^2}}}\right)+\frac{2\mu}{f^2+\frac{f^2}{-1+\sqrt{1+l_b^2 f^2}}}\,. \tag{5.36}$$

As expected, the integration of Eq. (5.36) between f_{min} and ∞ results in $E_{0l}/(1+\beta)$ when the large-loop approximations are applied.

The $\Omega_{GW} \propto f^{-1}$ behaviour which was mentioned in the small-loop regime is also present for large loops at very high frequencies. As explained before, for frequencies $f > f_{min}(t_i)$ the main contributors are loops at the end stages of their lives. The length of these loops decreases and they eventually enter the small-loop regime. Therefore, for sufficiently high frequencies the main contributors will be small loops and, from Eq. (5.15) with a constant lower bound on the integral, the $\Omega_{GW} \propto f^{-1}$ signature occurs. Notice that while for loops which are born small this behaviour happens for frequencies $f > f_{min}(t_i)$, for large loops this behaviour only takes place once they become small which happens for frequencies slightly higher that $f_{min}(t_i)$. This becomes apparent in Fig. 5.8, where this behaviour is shown to take place after $f_{min}(t_i)$ — depicted in dashed line — but not immediatly after as was the case for small-loops.

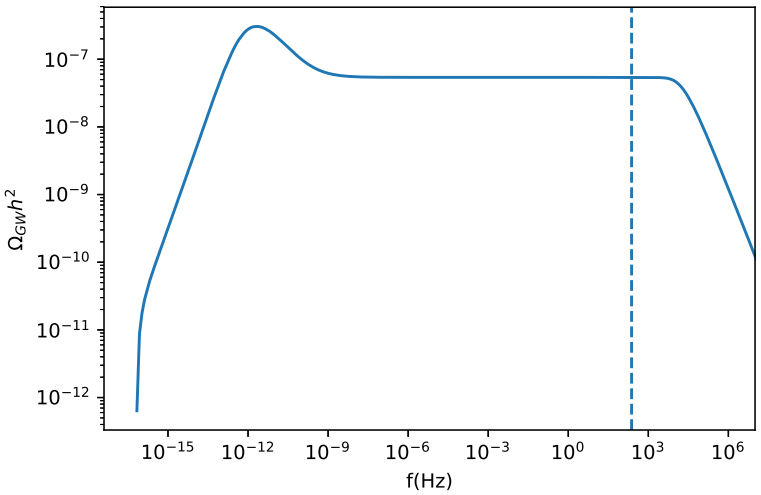

Figure 5.8: The SGWB spectrum produced by a network of cosmic strings with $\alpha = 10^{-1}$ and $G\mu = 10^{-7}$. The dashed line indicates the position of $f_{min}(t_i)$. For higher frequencies, the behaviour $\Omega_{GW} \propto f^{-1}$ is observed. The loop-chopping efficiency is set to $\tilde{c} = 0.23$.

5.2.1 Dependency on α

In the large-loop regime, larger loops (with higher α) live longer. Therefore, a part of their energy is emitted later, and suffers a smaller redshift. Consequently, networks with a higher α are expected to produce a SGWB spectrum with a higher amplitude.

This effect is observable in Fig. 5.9, where several SGWB spectra are illustrated for different values of α. There are some changes in the shape of the spectra, mainly in the form of the peak and thhe amplitude increases with a higher α.

5.2.2 Dependency on $G\mu$

As explained earlier, the value of $G\mu$ affects the spectrum density both directly and indirectly since the life-time of a loop is affected by the value of $G\mu$. In the large-loop regime the effect of decreasing $G\mu$ (increasing the life-time) is to cause a less pronounced decrease of the amplitude of the spectrum, and a change in the peak to higher frequencies. Moreover, the peak is less noticeable when compared to the value of the flat part of the spectrum. These effects can be seen in Fig. 5.10 where the SGWB spectra for networks with different values of $G\mu$ are depicted.

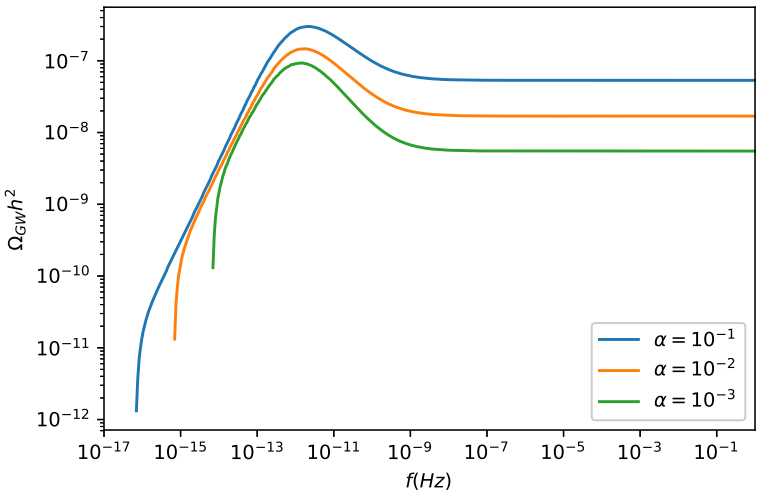

Figure 5.9: The SGWB spectra produced by a network of cosmic strings with $G\mu = 10^{-7}$ for different values of α, all in the large-loop regime. The loop-chopping efficiency is set to $\tilde{c} = 0.23$.

5.2.3 Equivalence to the literature

In the literature, the steps shown in this section regarding the computation of the SGWB spectrum for the large-loop regime are usually presented in a different, but equivalent, manner. Following Ref. [33], the authors show that the SGWB spectrum can be calculated as

$$\Omega_{\rm GW}(f) = \frac{16\pi}{3}\left(\frac{G\mu}{H_0}\right)^2 \frac{\Gamma}{f a_0^5}\int_{t_i}^{t_0} n\left(l(t'),t'\right) a^5(t') dt' \,, \tag{5.37}$$

where t_i is the instant of formation of the network, $n\left(l(t'),t'\right) dl$ is the number density of cosmic string loops with physical lengths between l and $l+dl$ at the time t and $l(t') = (2/f)(a(t')/a_0)$ is the physical length that cosmic string loops should have at a time t' to radiate GWs that have a frequency f at the present time. As Eq. (5.37) highlights, the loop distribution function, $n\left(l(t'),t'\right)$, is the pivotal quantity one has to characterize in order to compute the SGWB generated by cosmic string networks. Therefore, one needs to accurately estimate the size and number of cosmic string loops that exist at any instant in cosmic history in order to characterize their GW emission. Eq. (5.25) estimates the number density of loops that are created at any instant.

Since loops in the large-loop regime do not decay instantaneously, $n\left(l(t'),t'\right)$ has contribu-

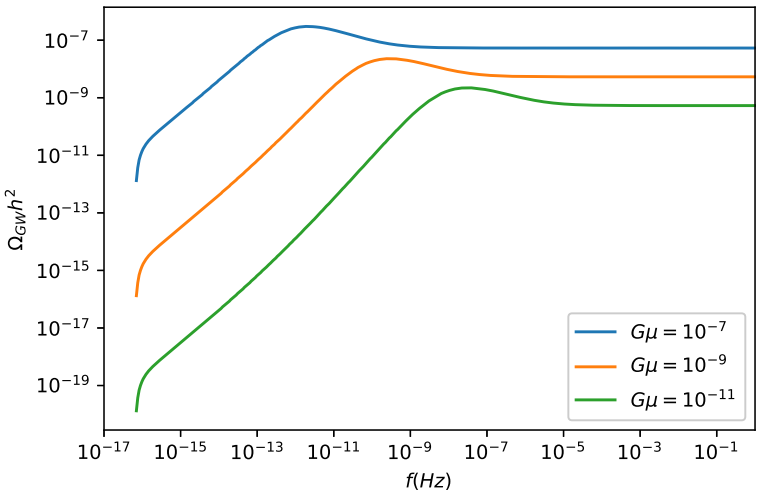

Figure 5.10: The SGWB spectra produced by a network of cosmic strings with $\alpha = 10^{-1}$ for different values of $G\mu$, all in the large-loop regime. The loop-chopping efficiency is set to $\tilde{c} = 0.23$.

tions from all pre-existing loops that have a physical length $l(t')$ at time t'. Determining the times of creation (t_b^i) of the loops that contribute to a given frequency — which one cannot do analytically if the networks are not in a linear scaling regime — is therefore the essential step in this computation. Given these instants, the number density of loops is given by [33]

$$n\left(l(t'), t'\right) = \sum_i \left\{ \frac{1}{\alpha \left.\frac{dL}{dt}\right|_{t=t_b^i} + \Gamma G\mu} \frac{\tilde{c}}{\alpha} \frac{\bar{v}(t_b^i)}{L^4(t_b^i)} \left(\frac{a(t_b^i)}{a(t')}\right)^3 \right\} . \tag{5.38}$$

Chapter 6

The SGWB spectrum produced by a network of i-strings

Several works predict the production of cosmic strings during or towards the end of an inflationary era [8, 41, 42, 43, 44, 45, 46]. In this chapter, we will investigate whether there is a specific gravitational wave signature generated by cosmic string networks produced during a primordial inflationary phase. These cosmic strings — which, for simplicity, we shall refer to as i-strings — are stretched and diluted as a result of the accelerated expansion of the cosmological background and, consequently, the characteristic length of the network grows very quickly. Thus, by the end of the inflationary phase, the characteristic length may be much larger than the Hubble radius, $LH \gg 1$. Therefore, while this condition holds, the network evolves according to the stretching regime, studied in chapter 4.

From Figs. 4.4a, 4.4b and 4.4c, it has been shown that $\bar{v}$ is close to zero while $LH \gg 1$, implying that the production of loops is suppressed in the stretching regime. However, these figures also show that the stretching regime is transient and the linear scaling regime is attained at a later time, when compared to a standard network of strings — a network which is created in the early Universe, after inflation. In fact, since $L \propto a$ in the stretching regime, one can see that for $0 < \beta < 1$ (as is the case in the radiation and matter eras), $LH \propto t^{\beta-1}$ decreases with physical time. Consequently, the characteristic length eventually becomes of the order of the Hubble radius and afterwards the network evolves towards its standard evolution. Only near

$LH = 1$ — which we will call the entry time — does the network start producing a significant amount loops and emitting a significant amount of gravitational waves. The sooner the network is created in the inflationary phase, the more it suffers an accelerated expansion and the larger its characteristic length is at the end of inflation. This results in a later entry time as evidenced by Fig. 4.4a.

6.1 Signature in the SGWB spectrum produced by i-strings

Since the general effect of experiencing an inflationary phase is to delay the onset of (significant) cosmic string loops production, one may then expect the SGWB spectrum generated by i-strings to be similar to an artificial spectrum produced by a network of strings created near the entry time. This is illustrated in Fig. 6.1 where the SGWB spectrum produced by i-strings with a scale factor at entry time $a_e = 10^{-16}$ is plotted along an artificial spectrum produced by a cosmic string network created (in scaling) at the time of entry, $a_c = 10^{-16}$. As predicted, both spectra are very similar and coincide with the standard spectrum in the low frequency range. Note, however, that there are significant differences in the approach to the standard spectrum: in the case of i-strings, after the entry time, the network approaches the scaling regime, while the network created at the entry time is modeled to already be in the scaling regime upon formation. After the approach to the linear scaling regime, both networks produce loops at an equal rate, giving rise to the same spectra for lower frequencies as a result. At higher frequencies, both spectra present the $\Omega_{GW} \propto f^{-1}$ behaviour as a consequence of the lack of production of loops which would contribute dominantly in this frequency range. As explained in chapter 5, this signature is produced by loops at the end of their lives, when they have already entered the small-loop regime. One can then conclude that the main signature of i-strings is to move this $\Omega_{GW} \propto f^{-1}$ behaviour to lower frequencies than those for which this signature would be observed in a standard SGWB spectrum.

Fig. 6.2 shows the SGWB spectrum produced by networks of i-strings with different entry times and also a standard spectrum for comparison. The $\Omega_{\rm GW}(f) \propto f^{-1}$ signature is observed in all cases. Fig. 6.2 illustrates that a later entry time results in a departure from the standard spectrum at lower frequencies. This is to be expected since a later entry time results in a

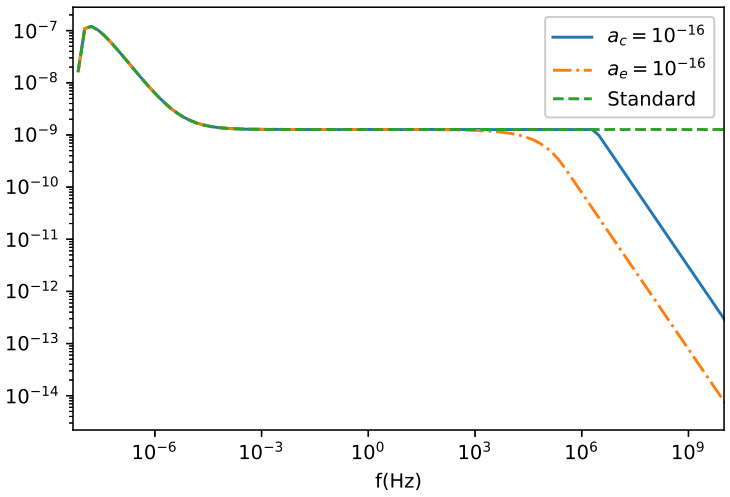

Figure 6.1: The SGWB spectrum, $\Omega_{GW}h^2$, as a function of frequency, f, for a network of i-strings with $a_e = 10^{-16}$ in the orange dash-dotted line and for a network created at $a_c = 10^{-16}$. The standard spectrum is depicted in the dashed line. The spectra were calculated with $\alpha = 10^{-9}$, $G\mu = 10^{-7}$ and $\tilde{c} = 0.23$.

longer delay of significant loop production, which means that the created loops will contribute dominantly to lower frequencies.

In Figs. 6.3 and 6.4 the spectra for i-string networks with $a_e = 10^{-10}$ is shown, for different values of α and $G\mu$ respectively. Within Fig. 6.3, the cases for which the formed loops are considered large ($\alpha \gg \Gamma G\mu$) are depicted in Fig. 6.3a and Fig. 6.3b shows the cases in which the loops are considered small upon formation. The $\Omega_{GW}h^2 \propto f^{-1}$ signature is produced by loops at the end of their lives, already in the small-loop regime regardless of their initial size, which explains why the behaviour is observed in every case for both figures. The dependence of α in the SGWB spectrum has been studied, and we concluded that in the regime of large loops, a larger α corresponds to a larger amplitude in the SGWB spectrum. Together with the fact that for a larger α the spectrum departs from the standard one at a lower frequency — since f_{min} of the first produced loops is lower — this results in the $\Omega_{GW}h^2 \propto f^{-1}$ signature almost coinciding for all cases. In the case of small loops this is not true because a change in α results in a shift of the spectrum in the frequency axis which is observed in Fig. 6.3b.

Fig. 6.4 once again shows that the signature $\Omega_{GW}h^2 \propto f^{-1}$ is present in every case. The distinction between large and small regimes is also present: the two spectra with lower

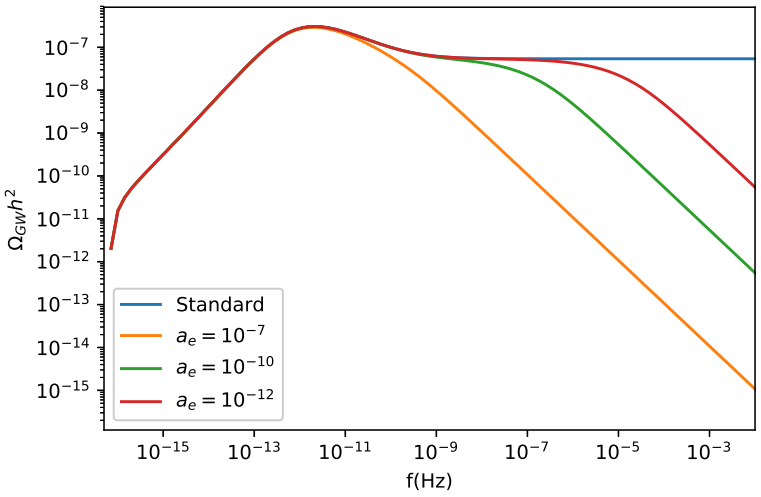

Figure 6.2: The SGWB spectrum, $\Omega_{GW}h^2$, as a function of frequency, f, for networks with different entry times. The spectra were calculated with $\alpha = 0.1$, $G\mu = 10^{-7}$ and $\tilde{c} = 0.23$.

amplitudes are cases in which the formed loops are considered large and therefore the signature coincides in these cases.

6.2 Observational implications

The $\Omega_{GW}h^2 \propto f^{-1}$ behaviour present at high frequencies in the SGWB spectrum produced by i-strings has important consequences when analyzing observational data. Since this signature implies a deficit of energy density at a specific range of frequencies, the absence of detection of the predicted SGWB spectrum for specific parameters within this frequency range, may indicate that the network went through a period of accelerated inflation instead of the immediate conclusion that it does not exist. Fig. 6.5 illustrates a case in which this may happen: the observational window of an experiment can coincide with the region of the $\Omega_{GW}h^2 \propto f^{-1}$ signature, preventing the detection of the SGWB spectrum. This implies that a network of i-strings can evade current constraints determined by gravitational experiments [43].

Fig. 6.5 depicts another interesting situation in which experiment 1 detects the standard SGWB spectrum at low frequencies, but experience 2, focused on higher frequencies, misses the predicted spectrum due to the $\Omega_{GW}h^2 \propto f^{-1}$ signature. For instance, looking at Fig. 2.4 , where the predicted observational window of experiments was shown, this situation may

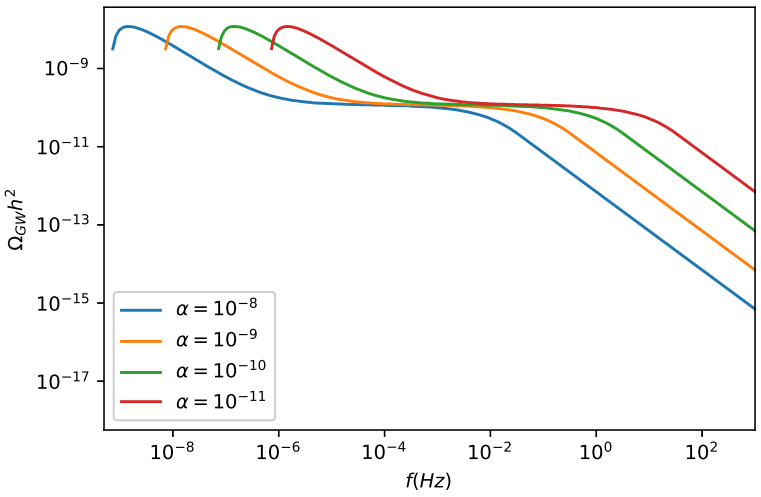

(a)

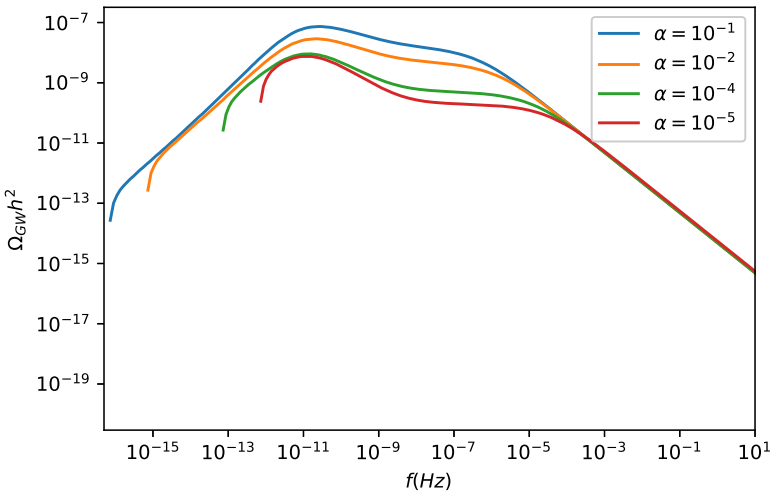

(b)

Figure 6.3: The SGWB spectrum, $\Omega_{GW}h^2$, as a function of frequency, f, for networks with different values of α. In the top pannel, cases where loops are consdered large are showed while in the bottom pannel cases in the small loop regime are plotted. The entry time is $a_e = 10^{-10}$ and the spectra were calculated with $G\mu = 10^{-8}$ and $\tilde{c} = 0.23$.

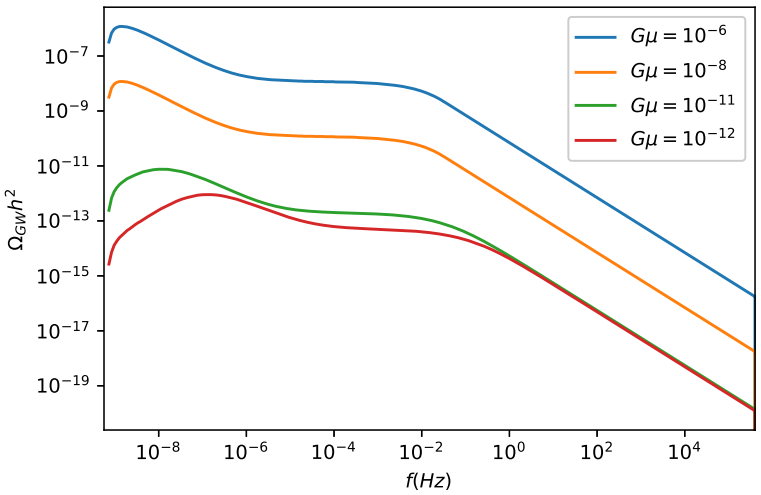

Figure 6.4: The SGWB spectrum, $\Omega_{GW}h^2$, as a function of frequency, f, for networks with different values of $G\mu$. The entry time is $a_e = 10^{-10}$ and the spectra were calculated with $\alpha = 10^{-8}$ and $\tilde{c} = 0.23$.

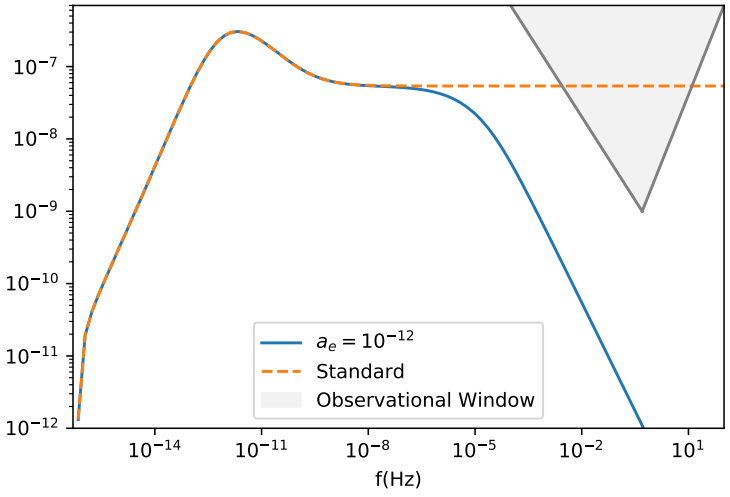

Figure 6.5: The SGWB spectrum, $\Omega_{GW}h^2$, as a function of frequency, f, for a standard network (in orange dashed line) and for a network of i-strings with $a_e = 10^{-12}$ (in solid blue line), both calculated with $\tilde{c} = 0.23$. The shaded area represents the observational window of an experimental apparatus that misses the SGWB spectrum due to the $\Omega_{GW} \propto f^{-1}$ signature. Note that this is merely illustrative and does not correspond to any specific experiment.

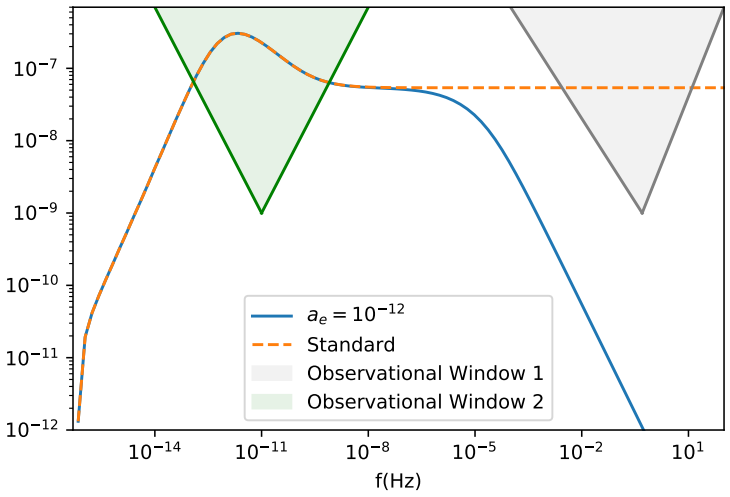

Figure 6.6: The SGWB spectrum, $\Omega_{GW}h^2$, as a function of frequency, f, for a standard network (in orange dashed line) and for a network of i-strings with $a_e = 10^{-12}$ (in solid blue line), both calculated with $\tilde{c} = 0.23$. The shaded areas represents the observational window of two different experimental apparatus. The first one detects the SGWB spectrum while the second one misses it due to the $\Omega_{GW} \propto f^{-1}$ signature. Note that these are merely illustrative and do not correspond to any specific experiment.

take place with pulsar timing arrays, such as the SKA, which is predicted to observe at lower frequencies, and with LISA, which will observe at higher frequencies.

On the other hand, forthcoming experiments may detect the $\Omega_{GW}h^2 \propto f^{-1}$ behaviour: if so, one would ask whether this is a specific signature of a primordial inflationary era.

6.2.1 Specificity of the inflation signature

We have shown that a $\Omega_{GW}h^2 \propto f^{-1}$ signature in the SGWB spectrum produced by i-strings is imprinted by the loops produced by the string network with the smallest comoving length.

One may therefore ask whether or not the observation of a smooth $\Omega_{GW}h^2 \propto f^{-1}$ high frequency cut-off to an otherwise standard SGWB cosmic string spectrum should be taken as a specific signature of inflation. As we have seen in Chapter 5, the (very) high frequency portion of any cosmic string SGWB spectrum — to which loops contribute in the end stages of their life — is generally expected to generate a signature of the same kind. This question then reduces to whether these two signatures may be distinguished.

To answer this question let us consider the signature generated by a (standard) cosmic string network produced at a temperature T_c in a string-forming phase transition ocurring after inflation in the early Universe. From Eq. (4.17), time of string formation is given by

$$t_c \sim (gG\mu)^{-1} m_{pl}^{-1} \sim (gG\mu)^{-1} t_{pl}\,, \tag{6.1}$$

where $g = 4\pi(\pi\mathcal{N}/45)^{1/2}$. Here, we have used the Friedmann equation $H^2 = 8\pi G\rho/3$ and taken into account the fact that in the radiation era $H = (2t)^{-1}$ and $\rho = \pi^2\mathcal{N}T^4/30$, where $\mathcal{N}$ is the number of effective relativistic degrees of freedom. We have also used natural units with $\hbar = c = k_B = 1$, so that Planck mass is given by $m_{pl} = t_{pl}^{-1} = G^{-1/2}$.

Considering that the initial friction dominated phase is transient and precedes the frictionless regime already studied, the first loops produced by the network generate gravitational waves whose frequency measured at the present time can be estimated to be

$$f > t_c^{-1}\,\frac{a_c}{a_0} \sim G\mu\, t_{pl}^{-1}\,\frac{a_c}{a_0}\,, \tag{6.2}$$

with

$$\frac{a_c}{a_0} \sim \frac{T_0}{T_c} \sim (G\mu)^{-1/2}\frac{T_0}{m_{pl}} \sim 2\times 10^{-32}(G\mu)^{-1/2}\,, \tag{6.3}$$

where $T_0 = 2.726\,\mathrm{K}$ is the observed cosmic microwave background temperature [47]. Here we have also assumed that these loops are created with the largest possible size, given by $\alpha \sim 1$, since we are interested in computing the lower limits for the frequency at which the initial $\Omega_{GW}h^2 \propto f^{-1}$ signature occurs. Loops with smaller size would contribute at even higher frequencies.

Hence, the $\Omega_{GW}h^2 \propto f^{-1}$ cut-off associated to a cosmic string network produced at a string-forming phase transition occurring after inflation only appears at frequencies

$$f > 4\times 10^{11}(G\mu)^{1/2}\,\mathrm{Hz}\,, \tag{6.4}$$

where we have taken into account that $t_{pl} = 5\times 10^{-44}\,\mathrm{s}$. For pulsar-timing experiments — which currently provide the stringest limits on the cosmic string SGWB — the $\Omega_{GW}h^2 \propto f^{-1}$ signature generated by cosmic string networks created after inflation would be within their

frequency range (roughly $10^{-9} - 10^{-6}\,\mathrm{Hz}$) for $G\mu \lesssim 10^{-41}$. This is far beyond the current reach of these experiments and, therefore, such a signature cannot be detected. The same is also true for the LIGO interferometer, which would only be able to detect this signature for $G\mu \lesssim 10^{-16}$. Moreover, one should not even expect the upcoming LISA interferometer to detect such a signature in spite of the significant increase in sensitivity it is expected to bring: this signature would only fall into its sensitivity window ($\sim 10^{-5} - 1\,\mathrm{Hz}$) for $G\mu \lesssim 10^{-23}$, which is also beyond its expected reach. This implies that either the value of $G\mu$ is small and there is insufficient power for this part of the spectrum to be observed with current or forecoming gravitational wave experiments, or this $\Omega_{GW}h^2 \propto f^{-1}$ signature will be outside the frequency range covered by these experiments.

Hence, we conclude that the observation with current or forthcoming experiments of a smooth transition between a standard SGWB cosmic string spectrum and a $\Omega_{GW}h^2 \propto f^{-1}$ spectrum would indeed provide strong evidence for a cosmic string network generated during a primordial inflationary era and would therefore provide evidence of such an era.

Although this signature is associated with inflation, we should note that it does not distinguish between different inflationary scenarios nor does it differentiate inflation from possible alternatives. Strictly speaking, the $\Omega_{GW}h^2 \propto f^{-1}$ signature should more precisely be seen as an evidence that the characteristic lengthscale of the network was larger than the Hubble radius in the past.

6.3 Recipe for the construction of spectrum

In this section we will provide a recipe to approximately construct the SGWB spectrum produced by a network of i-strings.

We start with a standard spectrum and determine a specific frequency, f_{cut}, dividing it in two regions: for $f < f_{cut}$, the standard spectrum holds; while for $f > f_{cut}$, it becomes a line of constant slope -1 (with $\Omega_{GW}h^2 \propto f^{-1}$), which intersects the standard spectrum at f_{cut}. This procedure is illustrated in Fig. 6.7. The spectrum produced by a network of i-strings is represented by the dash-dotted line and our approximation — which has a single parameter, f_{cut} — by the solid line.

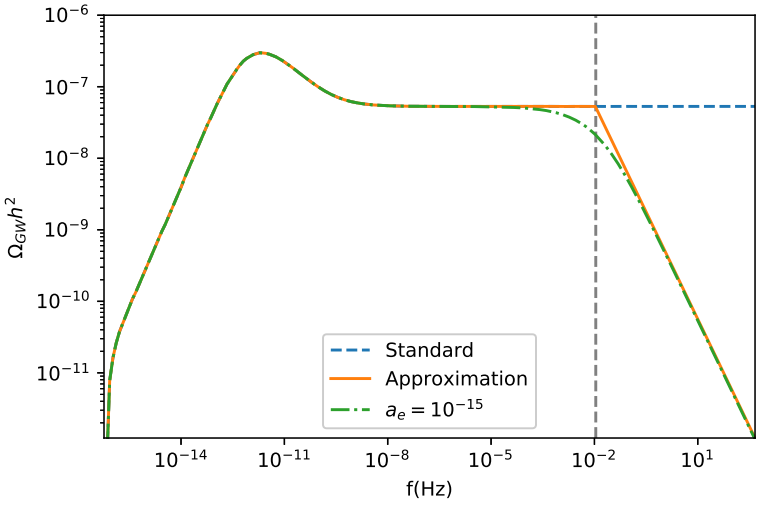

Figure 6.7: Aproximation (solid line) of the SGWB spectrum, $\Omega_{GW}h^2$, as a function of frequency, f, following the recipe developed in this section. The dash-dotted line represents the SGWB spectrum of network of i-strings, with $a_e = 10^{-15}$ and the dashed line represents the standard SGWB spectrum. For low frequencies, these 3 spectra coincide. The vertical dashed line indicates the position of f_{cut}. The loop size parameter was set to $\alpha = 0.1$ and $G\mu = 10^{-7}$. The loop-chopping efficiency parameter was set to $\tilde{c} = 0.23$.

From Fig. 6.7, it should be noted that, while the approximation is accurate for the most part of the spectrum, the sudden transition from the standard spectrum to a straight line results in a slight overestimation of the amplitude of the spectrum for frequencies near f_{cut}. However, for the purpose of deriving observational constraints, such an overestimation is not problematic: the resulting constraints will be safe, although a bit conservative.

The value of f_{cut} is estimated through a numerical fit, to take into account the two effects responsible for the way the $\Omega_{GW}h^2 \propto f^{-1}$ signature is added to an otherwise standard SGWB spectrum: the approximation to the linear scaling regime and the initial size of the loops — since this signature is associated with the small loop behaviour.

6.3.1 Case of small loops

Studying loops which are created already in the small-loop regime, we can isolate the first effect, the approach to the scaling regime. As seen in the evolution of $\bar{v}$, shown in Fig. 4.4c, one expects the network to start producing a significant amount of loops — and therefore emitting a significant amount of gravitational waves — near the entry time. However, by the

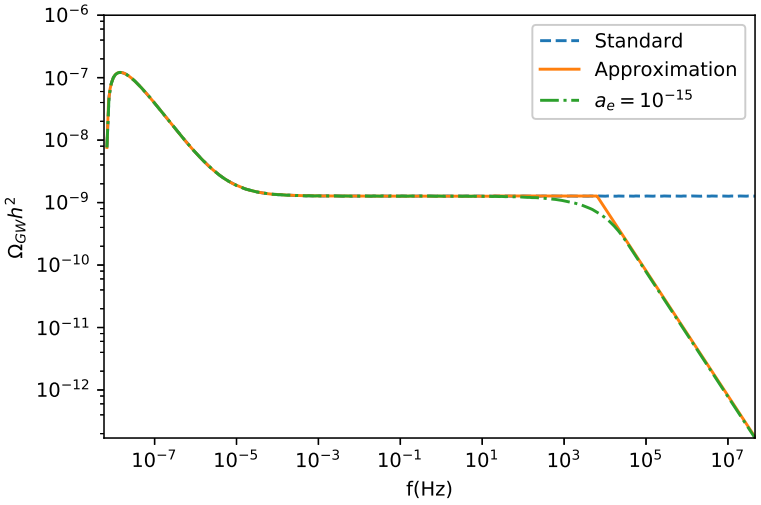

Figure 6.8: Aproximation (solid line) of the SGWB spectrum, $\Omega_{GW}h^2$, as a function of frequency, f, following the recipe developed in this section. The dash-dotted line represents the SGWB spectrum of network of i-strings, with $a_e = 10^{-15}$ and the dashed line represents the standard SGWB spectrum. The loop size parameter was set to $\alpha = 10^{-9}$ and $G\mu = 10^{-7}$. The loop-chopping efficiency parameter was set to $\tilde{c} = 0.23$.

entry time the network is not yet in a linear scaling regime (the value of $\bar{v}$ is approaching the scaling constant from below). This progression to the linear scaling regime results in a smooth transition from a standard spectrum to a region where $\Omega_{GW}h^2 \propto f^{-1}$, as was seen in a previous section, in Fig. 6.2.

The value of f_{cut} which takes into account this effect and produces the best approximation following our recipe, was numerically estimated to be the f_{min} of loops created at $a_{e^*} = 24 \times a_e$, which corresponds to $LH = 0.211$ — as expected LH is of order unity and close to the scaling value. From Eq. (5.1) f_{cut} can then be calculated as:

$$f_{cut} = f_{min}(a_{e^*}) = \frac{9.48}{\alpha} H(a_{e^*}) \frac{a_{e^*}}{a_0} \,. \tag{6.5}$$

In Fig. 6.8 our approximation is plotted along in a SGWB spectrum generated by i-strings for an entry time of $a_e = 10^{-15}$, in the regime of small loops. The approximation accurately depicts the spectrum for a wide range of frequencies, except in a region near f_{cut}, where the overestimation that was mentioned in the beginning of this section can be seen in the sudden transition from the standard SGWB spectrum to a signature of $\Omega_{GW}h^2 \propto f^{-1}$.

6.3.2 Case of large loops

For large loops, the fact that the loops created at a_{e^*} only behave as small loops at a later time needs to be taken into account, since it is the small-loop behaviour that is responsible for the $\Omega_{GW}h^2 \propto f^{-1}$ signature. To calculate this new f_{cut} one has to define when does a loop behave as a small one. A loop can be considered to start behaving as a small one at the time t_s given by:

$$l(t_s) < C\Gamma G\mu t_s \,, \tag{6.6}$$

where C is a constant of order unity. For this particular recipe, the value of C which originates the best approximation was found to be $C = 0.6$. From this condition it follows that the time when a loop created at time t_{e^*} (corresponding to the scale factor a_{e^*}) behaves as a small loop, t_s, can be calculated as

$$t_s = \frac{1}{1.6\Gamma G\mu}\left[\frac{0.211\alpha}{H(a_{e^*})} + \Gamma G\mu t_{e^*}\right]. \tag{6.7}$$

Knowing this time, f_{cut} can be calculated following Eqs. (5.1) and (5.5) as

$$f_{cut} = \frac{2}{\frac{0.211\alpha}{H(a_{e^*})} - \Gamma G\mu(t_s - t_{e^*})}\frac{a_s}{a_0}\,. \tag{6.8}$$

The calculation of f_{cut} should be done following Eq. (6.8) if $\alpha > 2.84\Gamma G\mu t_{e^*}H(a_{e^*})$. Otherwise, $t_s = t_{e^*}$ and Eq. (6.8) reduces to Eq. (6.5).

Fig. 6.7 shows this approximation applied to a case in which the loops are large, with $\alpha = 0.1$ and $G\mu = 10^{-7}$. In this case we are clearly in the large-loop regime and the approximation accurately depicts the signature of $\Omega_{GW}h^2 \propto f^{-1}$. The overestimation is restricted to a region around f_{cut}.

A case near the transition between what is considered a small or a large loop for this recipe is shown in Fig. 6.9. In this case we considered $\alpha = 10^{-9}$ and $G\mu = 10^{-7}$. Despite working better for cases which are clearly in the small- or large-loop regimes, this approximation can still be used for cases in the transition between these regimes — with only minor deviations in the high-frequency range— as evidenced by Fig. 6.9. It is important to note that this transition was defined for this recipe in particular.

This recipe provides a better fit for networks which reenter the Hubble radius during the

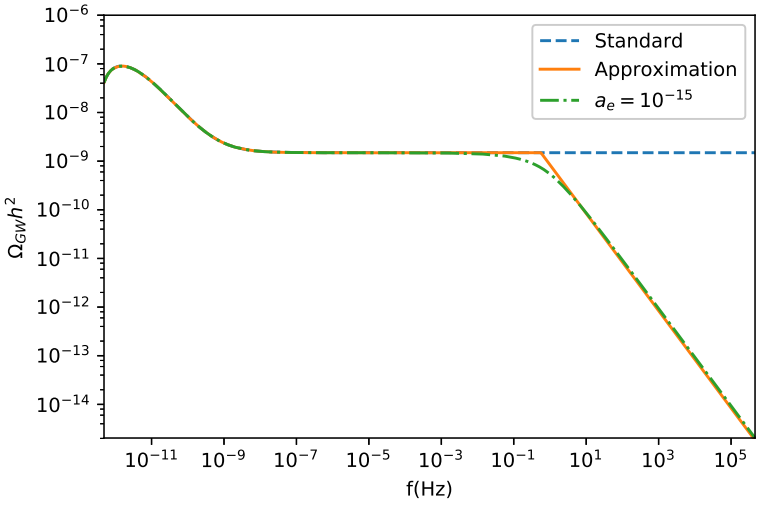

Figure 6.9: Aproximation (solid line) of the SGWB spectrum, $\Omega_{GW}h^2$, as a function of frequency, f, following the recipe developed in this section. The dash-dotted line represents the SGWB spectrum of network of i-strings, with $a_e = 10^{-15}$ and the dashed line represents the standard SGWB spectrum. The loop size parameter was set to $\alpha = 2 \times 10^{-5}$ and $G\mu = 10^{-7}$. The loop-chopping efficiency parameter was set to $\tilde{c} = 0.23$.

radiation era, since the SGWB of standard networks is constant in this era during which the network evolves in a scale-invariant manner. The matter era may not be long enough for the network to reach scaling. However, this recipe can also be used when the reentry occurs during the matter epoch, as shown in Fig. 6.10 — where the departure from the standard spectrum happens near the peak. Given that f_{cut} is not located in the plateau of the spectrum (see Fig. 6.10), the overestimation may be greater. However, even in this case the recipe may still be used to derive safe observational constraints.

From Eq. (5.11) it becomes evident that it is straigthforward to extend this approximation for any arbitrary harmonic mode of emission j. To do so one only needs to calculate f_{cut} following the recipe described in this section and multiply it by j. Furthermore, following Eq. (5.9), one can construct the final spectrum including as many modes as intended.

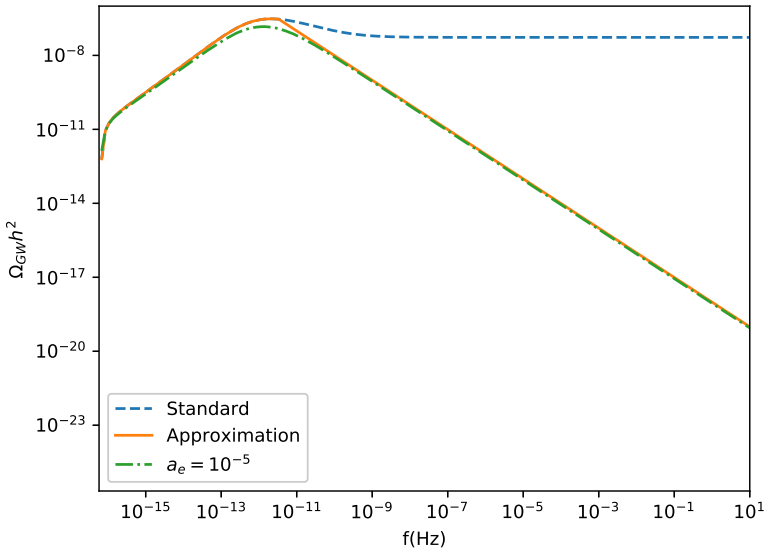

Figure 6.10: Aproximation (solid line) of the SGWB spectrum, $\Omega_{GW}h^2$, as a function of frequency, f, following the recipe developed in this section. The dash-dotted line represents the SGWB spectrum of network of i-strings, with $a_e = 10^{-5}$ and the dashed line represents the standard SGWB spectrum. The loop size parameter was set to $\alpha =$ and $G\mu = 10^{-7}$. The loop-chopping efficiency parameter was set to $\tilde{c} = 0.23$.

Chapter 7

Conclusions

The detection of cosmological topological defects would give us a profound insight into the early Universe, providing us with information about the phase transition that originated them. The recently inagurated area of gravitational wave astronomy serves as a new tool to probe possible observable signatures of these defects.

In this thesis we have explored the evolution of cosmic string networks and the production of the Stochastic Gravitational Wave Background (SGWB) that may be detected by current or future experiments. We computed this SGWB spectrum for several parameters, in the small- and large-loop regimes. We also focused on the possibility that cosmic string networks are created during an early inflationary phase — for simplicity, we defined these as i-string networks.

Using the Velocity-dependent One Scale (VOS) model to describe the dynamics of the network, i-string networks were shown to enter a transient stretching regime during inflation in which the production of closed loops and the emission of gravitational waves are significantly suppressed, and the characteristic size of the network becomes much larger than the Hubble radius. Standard evolution is delayed until the characteristic length becomes again smaller or of the order of the Hubble radius after inflation. We have shown that this delay is responsible for a specific high-frequency signature of the form $\Omega_{GW} \propto f^{-1}$ (the larger the delay is — or, equivalently, the earlier the network is created during inflation — the lower the frequency f_{cut} at which this signature appears). We further argued that this signature, if observed by current or forthcoming experiments on an otherwise standard SGWB spectrum, would provide strong

evidence for i-strings and, therefore, for (early) inflation.

In this work we also presented a simple single-parameter algorithm that allows for the construction of the SGWB spectrum produced by i-strings by using the spectrum of standard networks as a starting point and without the need for a full recomputation. This algorithm provides an accurate approximation of the i-string SGWB spectrum for a wide range of parameters, including the case of networks which only start producing a significant amount of gravitational waves in the matter dominated era.

Since the i-string SGWB signature corresponds to a deficit in power at high frequencies, it is possible that the lack of observation of the SGWB with current gravitational wave experiments might be associated to this deficit rather than a low value of $G\mu$. Therefore, it would be interesting in a future work to determine the observational constraints to be obtained by forthcoming gravitational wave experiments, or revise current cosmic strings constraints (in particular, on the value of $G\mu$) to include the extra-parameter f_{cut}, using the algorithm developed in this work.

Future work could also include an improvement of the algorithm, particularly by developing a fit specifically for when the reentry time of i-strings takes place during the matter era.

Bibliography

[1] A. Vilenkin and E. Shellard, *Cosmic strings and other topological defects*. Cambridge monographs on mathematical physics. Cambridge University Press, 2000.

[2] T. W. B. Kibble, *Phase transitions: Cosmology in the laboratory*, *Nature* **317** (Oct., 1985) 472.

[3] Y. Nambu, *Proceedings of int. conf. on elementary particles*, *Publications Office, Progress in Theoretical Phyisics, Kyoto* (1966).

[4] A. Vilenkin, *Cosmic defects*, in *Critical dialogues in cosmology. Proceedings, Celebration of the 250th Anniversary of Princeton University, Princeton, USA, June 24-27, 1996*, pp. 415–419, 1996. astro-ph/9610125.

[5] **Virgo, LIGO Scientific** Collaboration, B. P. Abbott *et. al.*, *Observation of Gravitational Waves from a Binary Black Hole Merger*, *Phys. Rev. Lett.* **116** (2016), no. 6 061102, [arXiv:1602.0383].

[6] J. J. Blanco-Pillado, K. D. Olum, and X. Siemens, *New limits on cosmic strings from gravitational wave observation*, *Phys. Lett.* **B778** (2018) 392–396, [arXiv:1709.0243].

[7] A. Vilenkin, *Gravitational radiation from cosmic strings*, *Phys. Lett.* **107B** (1981) 47–50.

[8] Q. Shafi and A. Vilenkin, *Spontaneously broken global symmetries and cosmology*, *Phys. Rev. D* **29** (Apr, 1984) 1870–1871.

[9] C. J. Hogan and M. J. Rees, *Gravitational interactions of cosmic strings*, *Nature* **311** (1984) 109–113. [,128(1984)].

[10] G. S. F. Guedes, P. P. Avelino, and L. Sousa, *Signature of inflation in the stochastic gravitational wave background generated by cosmic string networks*, *ArXiv e-prints* (2018) [arXiv:1809.1080].

[11] J. C. Mather *et. al.*, *A Preliminary measurement of the Cosmic Microwave Background spectrum by the Cosmic Background Explorer (COBE) satellite*, *Astrophys. J.* **354** (1990) L37–L40.

[12] R. P. Kirshner, *Hubble's diagram and cosmic expansion*, *Proceedings of the National Academy of Sciences* **101** (2004), no. 1 8–13, [http://www.pnas.org/content/101/1/8.full.pdf].

[13] **Planck** Collaboration, P. A. R. Ade *et. al.*, *Planck 2015 results. XIII. Cosmological parameters*, *Astron. Astrophys.* **594** (2016) A13, [arXiv:1502.0158].

[14] S. M. Carroll, *Lecture notes on general relativity*, December, 1997.

[15] J. Rosa, *Introduction to cosmology: lectures*, June, 2012.

[16] E. W. Kolb and M. S. Turner, *The Early Universe*, *Front. Phys.* **69** (1990) 1–547.

[17] D. Baumann, *Inflation*, in *Physics of the large and the small, TASI 09, proceedings of the Theoretical Advanced Study Institute in Elementary Particle Physics, Boulder, Colorado, USA, 1-26 June 2009*, pp. 523–686, 2011. arXiv:0907.5424.

[18] L. Blanchet, S. Kopeikin, and G. Schaefer, *Gravitational radiation theory and light propagation*, *Lect. Notes Phys.* **562** (2001) 141–166, [gr-qc/0008074]. [,141(2000)].

[19] P. Amaro-Seoane *et. al.*, *Laser Interferometer Space Antenna*, *ArXiv e-prints* (Feb., 2017) [arXiv:1702.0078].

[20] C. J. Moore, R. H. Cole, and C. P. L. Berry, *Gravitational-wave sensitivity curves*, *Class. Quant. Grav.* **32** (2015), no. 1 015014, [arXiv:1408.0740].

[21] B. Allen and E. P. S. Shellard, *Cosmic-string evolution: A numerical simulation*, *Phys. Rev. Lett.* **64** (Jan, 1990) 119–122.

[22] D. P. Bennett and F. m. c. R. Bouchet, *Evidence for a scaling solution in cosmic-string evolution*, *Phys. Rev. Lett.* **60** (Jan, 1988) 257–260.

[23] A. Albrecht and N. Turok, *Evolution of cosmic string networks*, *Phys. Rev. D* **40** (Aug, 1989) 973–1001.

[24] C. J. A. P. Martins and E. P. S. Shellard, *Extending the velocity dependent one scale string evolution model*, *Phys. Rev.* **D65** (2002) 043514, [hep-ph/0003298].

[25] C. J. A. P. Martins and E. P. S. Shellard, *Quantitative string evolution*, *Phys. Rev.* **D54** (1996) 2535–2556, [hep-ph/9602271].

[26] D. P. Bennett, *Evolution of cosmic strings*, *Phys. Rev. D* **33** (Feb, 1986) 872–888.

[27] D. P. Bennett, *Evolution of cosmic strings. ii*, *Phys. Rev. D* **34** (Dec, 1986) 3592–3607.

[28] B. Allen and R. R. Caldwell, *Small-scale structure on a cosmic-string network*, *Phys. Rev. D* **43** (May, 1991) 3173–3187.

[29] D. Austin, E. J. Copeland, and T. W. B. Kibble, *Evolution of cosmic string configurations*, *Phys. Rev.* **D48** (1993) 5594–5627, [hep-ph/9307325].

[30] J. N. Moore, E. P. S. Shellard, and C. J. A. P. Martins, *On the evolution of Abelian-Higgs string networks*, *Phys. Rev.* **D65** (2002) 023503, [hep-ph/0107171].

[31] C. J. A. P. Martins, J. N. Moore, and E. P. S. Shellard, *A Unified model for vortex string network evolution*, *Phys. Rev. Lett.* **92** (2004) 251601, [hep-ph/0310255].

[32] L. Sousa, *String and brane networks in higher dimensions*. phdthesis, Departamento de Física da Faculdade de Ciências da Universidade do Porto, Oct., 2011.

[33] L. Sousa and P. P. Avelino, *Stochastic Gravitational Wave Background generated by Cosmic String Networks: Velocity-Dependent One-Scale model versus Scale-Invariant Evolution*, *Phys. Rev.* **D88** (2013), no. 2 023516, [arXiv:1304.2445].

[34] P. P. Avelino and L. Sousa, *Domain wall network evolution in (N+1)-dimensional FRW universes*, *Phys. Rev.* **D83** (2011) 043530, [arXiv:1101.3360].

[35] J. M. Quashnock and D. N. Spergel, *Gravitational self-interactions of cosmic strings*, *Phys. Rev. D* **42** (Oct, 1990) 2505–2520.

[36] M. Hindmarsh, J. Lizarraga, J. Urrestilla, D. Daverio, and M. Kunz, *Scaling from gauge and scalar radiation in Abelian Higgs string networks*, *Phys. Rev.* **D96** (2017), no. 2 023525, [arXiv:1703.0669].

[37] R. R. Caldwell and B. Allen, *Cosmological constraints on cosmic string gravitational radiation*, *Phys. Rev.* **D45** (1992) 3447–3468.

[38] S. A. Sanidas, R. A. Battye, and B. W. Stappers, *Constraints on cosmic string tension imposed by the limit on the stochastic gravitational wave background from the European Pulsar Timing Array*, *Phys. Rev.* **D85** (2012) 122003, [arXiv:1201.2419].

[39] T. Vachaspati and A. Vilenkin, *Gravitational Radiation from Cosmic Strings*, *Phys. Rev.* **D31** (1985) 3052.

[40] L. Sousa and P. P. Avelino, *Stochastic gravitational wave background generated by cosmic string networks: The small-loop regime*, *Phys. Rev.* **D89** (2014), no. 8 083503, [arXiv:1403.2621].

[41] L. Kofman and A. Linde, *Generation of density perturbations in inflationary cosmology*, *Nuclear Physics B* **282** (1987) 555 – 588.

[42] K. Freese, T. Gherghetta, and H. Umeda, *Moduli inflation with large scale structure produced by topological defects*, *Phys. Rev.* **D54** (1996) 6083–6087, [hep-ph/9512211].

[43] K. Kamada, Y. Miyamoto, and J. Yokoyama, *Evading the pulsar constraints on the cosmic string tension in supergravity inflation*, *JCAP* **1210** (2012) 023, [arXiv:1204.3237].

[44] K. Kamada, Y. Miyamoto, D. Yamauchi, and J. Yokoyama, *Effects of cosmic strings with delayed scaling on CMB anisotropy*, *Phys. Rev.* **D90** (2014), no. 8 083502, [arXiv:1407.2951].

[45] A. D. Linde, *Axions in inflationary cosmology*, *Phys. Lett.* **B259** (1991) 38–47.

[46] A. D. Linde, *Hybrid inflation*, *Phys. Rev.* **D49** (1994) 748–754, [astro-ph/9307002].

[47] D. J. Fixsen, *The Temperature of the Cosmic Microwave Background*, *Astrophys. J.* **707** (2009) 916–920.